

## RESEARCH ARTICLE

# The centriolar satellite protein Cfap53 facilitates formation of the zygotic microtubule organizing center in the zebrafish embryo

Sven Willekers<sup>1</sup>, Federico Tessadori<sup>1</sup>, Babet van der Vaart<sup>2</sup>, Heiko H. Henning<sup>3</sup>, Riccardo Stucchi<sup>2,4</sup>, Maarten Altelaar<sup>4</sup>, Bernard A. J. Roelen<sup>5</sup>, Anna Akhmanova<sup>2</sup> and Jeroen Bakkers<sup>1,6,\*</sup>

## ABSTRACT

In embryos of most animal species, the zygotic centrosome is assembled by the centriole derived from the sperm cell and pericentriolar proteins present in the oocyte. This zygotic centrosome acts as a microtubule organizing center (MTOC) to assemble the sperm aster and mitotic spindle. As MTOC formation has been studied mainly in adult cells, very little is known about the formation of the zygotic MTOC. Here, we show that zebrafish (*Danio rerio*) embryos lacking either maternal or paternal Cfap53, a centriolar satellite protein, arrest during the first cell cycle. Although Cfap53 is dispensable for sperm aster function, it aids proper formation of the mitotic spindle. During cell division, Cfap53 colocalizes with  $\gamma$ -tubulin and with other centrosomal and centriolar satellite proteins at the MTOC. Furthermore, we find that  $\gamma$ -tubulin localization at the MTOC is impaired in the absence of Cfap53. Based on these results, we propose a model in which Cfap53 deposited in the oocyte and the sperm participates in the organization of the zygotic MTOC to allow mitotic spindle formation.

**KEY WORDS:** Ccdc11, Cfap53, Centriolar satellites, MTOC, Cell division, Maternal, Paternal, Zebrafish

## INTRODUCTION

The animal embryo must undergo multiple rounds of cell divisions to form a multicellular organism composed of hundreds of different cell types. During each cell division, microtubule organizing centers (MTOCs) participate in the formation of the mitotic spindle required to segregate the chromosomes into the two daughter cells. In dividing animal cells, the centrosome is the main MTOC. Centrosomes are composed of a pair of centrioles surrounded by a complex protein structure consisting of microtubule nucleating

and anchoring proteins called the pericentriolar material (PCM) (reviewed by Doxsey, 2001; Gould and Borisy, 1977).

In most animal oocytes, centrosomes are eliminated during oogenesis (Schatten et al., 1989; Szollosi et al., 1972). After fertilization, centrosomes are reassembled, which requires the interaction between the centrioles present in the sperm cell and maternal factors present in the oocyte (Holy and Schatten, 1997; Yabe et al., 2007). The sperm cell contains a pair of centrioles termed proximal and distal centrioles, but most centrosomal components are eliminated from the sperm cell (reviewed by Schatten, 1994; Sutoovsky and Schatten, 1999). Subsequently, after fertilization, the proximal centriole recruits centrosomal components that are deposited maternally in the oocyte to form a functional zygotic centrosome (reviewed by Schatten, 1994). One of the best characterized centrosomal components that is recruited to the MTOC after fertilization is  $\gamma$ -tubulin. It is part of the  $\gamma$ -tubulin ring complex ( $\gamma$ TuRC) that serves as a template for nucleating microtubules (reviewed by Kollman et al., 2011). How  $\gamma$ TuRC recruitment is facilitated towards the MTOC is still unclear. *In vitro* studies have shown that both microtubule-based active transport and passive diffusion contribute to centrosomal  $\gamma$ TuRC recruitment (Dammermann and Merdes, 2002; Félix et al., 1994; Khodjakov and Rieder, 1999; Moritz et al., 1998; Quintyne et al., 1999; Schnackenberg et al., 1998; Stearns and Kirschner, 1994; Young et al., 2000). In rodents, the sperm centriole is lost during spermatogenesis (Schatten et al., 1986; Woolley and Fawcett, 1973). However, MTOCs are still formed by recruitment of centrosomal components independently of centrioles (Gueth-Hallonet et al., 1993).

During early cleavage stages, zebrafish embryos have large MTOCs in which PCM components do not form a well-defined structure, but appear as cytoplasmic foci (Lindeman and Pelegri, 2012; Rathbun et al., 2020). This specific organization of the MTOC could support a mechanism that enables the mitotic spindle to span the large embryonic cells. The establishment of this unique MTOC after fertilization is probably highly coordinated and dependent on maternal and/or paternal factors present in the fertilized embryo.

Forward genetic screens in zebrafish are an unbiased approach to identify parental factors that have an important biological role in early development (Pelegri and Mullins, 2016). Several zebrafish and medaka mutants have been identified via this approach and proven to be very informative for the identification and characterization of some of these maternal and paternal factors (Abrams et al., 2020; Dekens et al., 2003; Inoue et al., 2017; Yabe et al., 2007). The zebrafish gene *cellular atoll* (*cea*) encodes for the centriole duplication factor Sas-6 (Yabe et al., 2007). Maternal *cea* (*sass6*) mutant embryos proceed through the first cell division but show mitotic defects from the second cell division onwards. Paternal *cea* mutant embryos have a delayed

<sup>1</sup>Hubrecht Institute-KNAW, Utrecht 3584 CT, The Netherlands. <sup>2</sup>Cell Biology, Neurobiology and Biophysics, Department of Biology, Faculty of Science, Utrecht University, Utrecht 3584 CH, The Netherlands. <sup>3</sup>Equine Sciences, Department Clinical Sciences, Faculty of Veterinary Medicine, Utrecht University, Utrecht 3584 CM, The Netherlands. <sup>4</sup>Biomolecular Mass Spectrometry and Proteomics, Bijvoet Center for Biomolecular Research and Utrecht Institute for Pharmaceutical Sciences, Utrecht University, Utrecht 3584 CH, The Netherlands. <sup>5</sup>Embryology, Anatomy and Physiology, Department Clinical Sciences, Faculty of Veterinary Medicine, Utrecht University, Utrecht 3584 CT, The Netherlands. <sup>6</sup>Department of Pediatric Cardiology, Division of Pediatrics, University Medical Center Utrecht, Utrecht 3584 EA, The Netherlands.

\*Author for correspondence (j.bakkers@hubrecht.eu)

© A.A., 0000-0002-9048-8614; J.B., 0000-0002-9418-0422

This is an Open Access article distributed under the terms of the Creative Commons Attribution License (<https://creativecommons.org/licenses/by/4.0>), which permits unrestricted use, distribution and reproduction in any medium provided that the original work is properly attributed.

Handling Editor: Steve Wilson  
Received 18 November 2020; Accepted 20 July 2022

first cell division, but cell division proceeds normally thereafter. The zebrafish gene *fruitless cycle* encodes the lymphoid-restricted membrane protein (Lrmp); in maternal *fue* (*lrmp*) mutant embryos, the male and female pronuclei fail to fuse (Dekens et al., 2003; Lindeman and Pelegri, 2012). In normal conditions, the two pronuclei fuse to one zygote nucleus in a process called nuclear congression. Nuclear congression requires the formation of a microtubule aster that nucleates from the proximal centriole and attaches to the pronuclei to bring them together, a process that fails in *fue* mutants (Dekens et al., 2003; Lindeman and Pelegri, 2012). In mouse embryos, nuclear congression appears different as it is facilitated by two bipolar spindles formed by two clusters of MTOCs around each pronucleus (Reichmann et al., 2018). The medaka (*Oryzias latipes*) maternal WD40 repeat-containing protein, Wdr8 (the orthologue of human WRAP73), is important during MTOC assembly (Inoue et al., 2017). Maternal zygotic *wdr8* (*wrap73*) mutant embryos form multipolar mitotic spindles resulting in chromosome alignment errors. With its WD40-containing domain, Wdr8 interacts with the centriolar satellite protein SSX2IP (Inoue et al., 2017). Additional maternal effect mutations that affect cell division in the early embryo have been identified via a recent forward genetic screen, expanding the molecular-genetic understanding of parental contribution in early embryonic development further (Abrams et al., 2020).

Centriolar satellites have been identified as non-membranous granules that surround the centrosomes (Dammermann and Merdes, 2002; Kubo et al., 1999; Odabasi et al., 2019; Prosser and Pelletier, 2020). The best known marker for centriolar satellites is PCMI as it is the first centriolar satellite protein that was identified (Balczon et al., 1994; Kubo et al., 1999; Kubo and Tsukita, 2003). Since then, many more proteins have been identified as components of centriolar satellites, including the cilia- and flagella-associated protein Cfap53 (also known as Ccdc11). Many of the identified centriolar satellites contain coiled-coil domains, including PCMI and Cfap53 (Balczon et al., 1994; Kubo et al., 1999; Silva et al., 2016).

To gain insight into the formation of the MTOC and the role of centriolar satellite proteins herein, we have studied the zebrafish *cfap53* mutant. We and others have previously shown that the zebrafish *cfap53* gene is expressed in ciliated organs of the embryo, including the Kupffer's vesicle, which is the zebrafish left-right organizer (Bakkers et al., 2009; Hirokawa et al., 2006). Zebrafish and mouse *cfap53/Cfap53* mutant embryos develop normally but show organ laterality defects due to compromised cilia function in the left-right organ, which resembles patients with homozygous *CFAP53* mutations (Ide et al., 2020; Narasimhan et al., 2015; Noël et al., 2016; Perles et al., 2012; Silva et al., 2016). Zebrafish homozygous *cfap53* mutants are adult viable and, in this study, we find that embryos lacking either maternal or paternal Cfap53 arrest in the first cell division. In the absence of Cfap53, the formation of the mitotic spindle is affected. We report that Cfap53 interacts with centriolar satellite proteins and centrosomal components, and plays a role in the localization of  $\gamma$ -tubulin to the zygotic MTOC. These findings reveal a novel role for maternal and paternal Cfap53 during zygotic MTOC formation in the zebrafish embryo.

## RESULTS

### Cfap53 has a maternal and paternal role in embryonic cell division

When homozygous *cfap53*<sup>-/-</sup> fish were crossed, we observed in independent crosses that 25-100% of the progeny did not develop

**Table 1. Effect of maternal and paternal loss of Cfap53 on embryo development**

Genotype	Pair	n	Developing embryos (%)	Arrested embryos (%)
Wild type ♀×wild type ♂	1	132	83	17
	2	55	95	5
	3	175	89	11
	4	47	96	4
<i>cfap53</i> <sup>-/-</sup> ♀× <i>cfap53</i> <sup>-/-</sup> ♂	1	106	71	29
	2	24	75	25
	3	188	53	47
	4	30	0	100
	5	13	8	92
<i>cfap53</i> <sup>-/-</sup> ♀×wild type ♂	1	62	71	29
	2	181	29	71
	3	248	46	54
	4	183	0	100
	5	108	51	49
Wild type ♀× <i>cfap53</i> <sup>-/-</sup> ♂	1	50	16	84
	2	65	51	49
	3	127	79	21
	4	40	23	78
	5	46	80	20

into normal embryos but instead arrested at the first cell cleavage with a single nucleus (Table 1). In time-lapse movies of these embryos lacking maternal (M) and paternal (P) *cfap53* (hereafter referred to as MP*cfap53*<sup>-/-</sup>) we observed temporarily invaginations of the cell membrane, but these never resulted in cell divisions (Fig. 1A,B). As we could not distinguish the MP*cfap53*<sup>-/-</sup> eggs before the first cell division we fixed MP*cfap53*<sup>-/-</sup> eggs at different stages after fertilization and stained nuclear DNA with DAPI (Fig. 1C,D). Although at 10 min post fertilization (mpf) and 20 mpf no differences were apparent, we observed at 30 mpf and 45 mpf that ~50% of MP*cfap53*<sup>-/-</sup> embryos displayed an aberrant and variable nuclear morphology with dispersed chromosomes and micronuclei (Fig. 1C,D: 30 mpf: n=8/17; 45 mpf: n=9/18). Importantly, the MP*cfap53*<sup>-/-</sup> embryos in which the first cell division did occur (Fig. 1A) developed normally and could be grown to viable and fertile adults. Interestingly, embryos derived from either homozygous *cfap53*<sup>-/-</sup> males or females crossed to an otherwise wild-type female or male, respectively, displayed the same arrest in the first cell division (Table 1). As unfertilized eggs arrest in a similar manner, we investigated whether the arrested *cfap53*<sup>-/-</sup> embryos were fertilized. We first analyzed sperm cell number and motility of *cfap53*<sup>-/-</sup> males, and did not observe any significant differences with sperm isolated from wild-type males (Fig. 2A,B, Table S1). Next, we analyzed whether DNA replication was initiated in MP*cfap53*<sup>-/-</sup> embryos, as this occurs only in fertilized eggs (Dekens et al., 2003). Indeed, we observed that EdU incorporation correlates well with fertilization as wild-type embryos incubated with EdU directly after fertilization and analyzed at 45 mpf (at the two-cell stage) efficiently incorporated EdU into their DNA (Fig. 2C and Table 2A; wild-type cross embryos at the two-cell stage, EdU<sup>+</sup>: n=23/23). This was in contrast to unfertilized (squeezed) eggs, as we never observed EdU incorporation in unfertilized eggs (Fig. 2C and Table 2A; unfertilized eggs, EdU<sup>+</sup>: n=0/23) as reported earlier (Dekens et al., 2003). In crosses from *cfap53*<sup>-/-</sup> pairs, we found that 53% of the arrested embryos had not incorporated the EdU, indicating that these were not fertilized or did not take up the EdU efficiently (Table 2A; *cfap53*<sup>-/-</sup> cross embryos at the one-cell stage, EdU<sup>+</sup>: n=29/55). Importantly, we observed that 47% of arrested MP*cfap53*<sup>-/-</sup> embryos efficiently incorporate

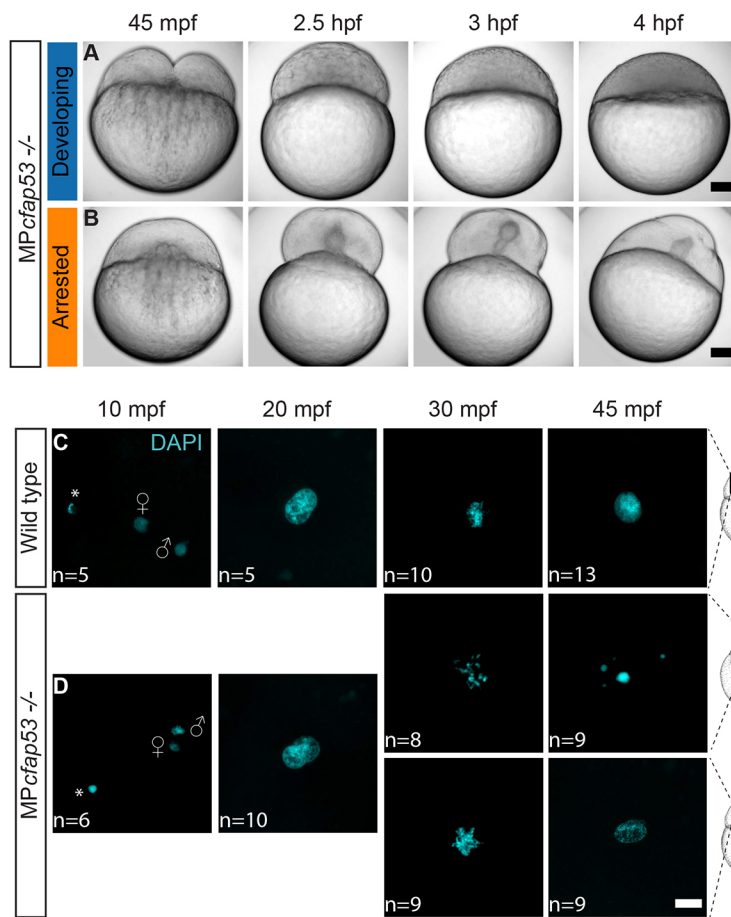


**Fig. 1. *MPcfap53<sup>-/-</sup>* embryos arrest and display aberrant nuclear morphology.** (A,B) Time series of maternal and paternal (MP)*cfap53<sup>-/-</sup>* embryos from 45 mpf up to 4 hpf. Although a small fraction of the *MPcfap53<sup>-/-</sup>* embryos displayed normal development (A,  $n=15$ ), most embryos arrested at the one-cell stage (B,  $n=52$ ). (C,D) Confocal images of wild-type (C) and *MPcfap53<sup>-/-</sup>* (D) embryos at indicated stages of development stained with DAPI to visualize nuclei, indicating that aberrant nuclear morphology starts to form at 30 mpf. Results were obtained from two different *cfap53<sup>-/-</sup>* pairs. Asterisks indicate polar bodies. Gender symbols indicate a male or female pro-nucleus. Scale bars: 100 μm in A,B; 20 μm in C,D. Schematics of embryonic development are adapted, with permission, from Kimmel et al. (1995).

EdU (Fig. 2C and Table 2A; *cfap53<sup>-/-</sup>* cross embryos at the one-cell stage,  $\text{EdU}^+$ :  $n=26/55$ ), demonstrating that these embryos, although being fertilized, failed to complete cytokinesis. As we observed the cell division arrest in embryos derived from either *cfap53<sup>-/-</sup>* males crossed with wild-type females or *cfap53<sup>-/-</sup>* females crossed with wild-type males, we also tested the EdU incorporation in such embryos. These embryos are referred to as *Pcfap53<sup>-/-</sup>* embryos (for lacking paternal *Cfap53*) and *Mcfap53<sup>-/-</sup>* embryos (for lacking maternal *Cfap53*). Importantly, EdU was incorporated in both *Pcfap53<sup>-/-</sup>* embryos and *Mcfap53<sup>-/-</sup>* embryos (Table 2a). The EdU incorporation was very efficient in *Pcfap53<sup>-/-</sup>* embryos ( $\text{EdU}^+$ :  $n=14/16$ ), which indicates that *cfap53<sup>-/-</sup>* sperm are very effective in fertilizing eggs. This is consistent with the observed normal sperm numbers and their motility. The EdU incorporation was less efficient for the *Mcfap53<sup>-/-</sup>* embryos ( $\text{EdU}^+$ :  $n=18/33$ ), suggesting a lower fertilization rate.

After fertilization, the male and female pronuclei come together during the nuclear congression, after which they fuse to form the zygotic nucleus. To analyze whether nuclear congression is affected in *MPcfap53<sup>-/-</sup>* embryos, we took clutches of *MPcfap53<sup>-/-</sup>* embryos and fixed some of the embryos at 15 mpf to analyze nuclear congression (Fig. 2D), while the rest of the clutch was analyzed live for cytokinesis (Fig. 2E). We analyzed at least three independent wild-type and *cfap53<sup>-/-</sup>* pairs, and found no significant difference in nuclear congression between *MPcfap53<sup>-/-</sup>* and wild-type embryos (Fig. 2D). Cytokinesis, however, was significantly less frequent in *MPcfap53<sup>-/-</sup>* embryos (Fig. 2E). These results indicate that nuclear congression is not affected in *MPcfap53<sup>-/-</sup>* embryos.

Next, we addressed whether DNA replication is continued in the *MPcfap53<sup>-/-</sup>* embryos in which cytokinesis failed, as was reported for *fue* mutants (Dekens et al., 2003). We therefore incubated embryos with EdU starting at 45 mpf and observed that 50% of the arrested *MPcfap53<sup>-/-</sup>* embryos still incorporated EdU (Table 2B; *cfap53<sup>-/-</sup>* cross embryos at the one-cell stage,  $\text{EdU}^+$ :  $n=22/44$ ). These results indicate that when cytokinesis fails in *MPcfap53<sup>-/-</sup>* embryos, DNA replication can continue resulting in endoreduplication. In summary, although maternal- and paternal-provided *Cfap53* is not required for nuclear congression, it facilitates karyokinesis and cytokinesis.

### Cfap53 interactome

Coiled-coil domain-containing proteins often act as scaffolds for large protein complexes, which is consistent with the observation that in cultured cells *Cfap53* protein localizes to centriolar satellites and is required for their integrity (Silva et al., 2016). To identify proteins that interact with *Cfap53*, we performed *Cfap53* protein pull downs followed by mass spectrometry (MS). Compared with cytoplasmic proteins, zebrafish embryos contain relatively large amounts of yolk proteins, which could hamper such an approach. We therefore expressed human CFPA53 fusion proteins [with N-terminal or C-terminal biotinylated GFP (bioGFP)] in HEK293 cells (Fig. S1). In HEK293 cells with low levels of BioGFP-CFPA53, the fusion protein localized to centrosomes, marked by  $\gamma$ -tubulin (Fig. S1). Streptavidin-based pull downs followed by MS resulted in the retrieval of in total 1148 proteins that were pulled down by both the bioGFP-CFPA53 and the CFPA53-bioGFP. For these two biological samples, the Pearson correlation of the MS



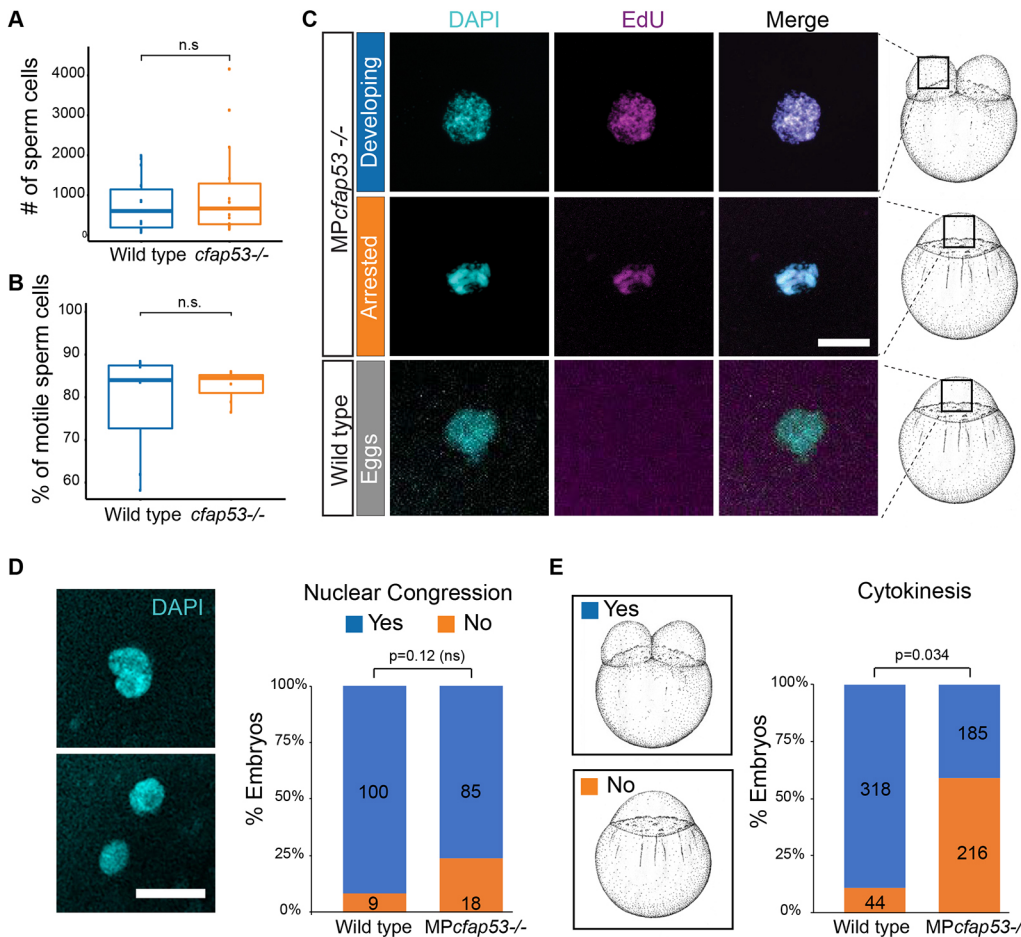


**Fig. 2. *cfap53*<sup>-/-</sup> fish are fertile.** (A,B) Boxplots for sperm cell analysis showing the total number (horizontal lines) of sperm cells counted (A) and percentage of motile sperm cells (B) in spermatozoa derived from wild type ( $n=7$ ) and *cfap53*<sup>-/-</sup> males ( $n=7$ ). Boxes indicate upper and lower quartiles and whiskers indicate upper and lower extremes. (C) Confocal images showing DAPI staining and EdU incorporation in MP*cfap53*<sup>-/-</sup> embryos and lack of EdU incorporation in unfertilized eggs. EdU incubation was performed from 0 to 60 mpf. Quantification of the results are presented in Table 2. (D) Confocal images of one-cell stage embryos stained with DAPI showing either lack of nuclear congression (bottom) or initiation of nuclear congression (top) of male and female pronuclei. Graph shows a quantification of observed nuclear congression in wild-type and MP*cfap53*<sup>-/-</sup> embryos. (E) Graph shows quantification of observed cytokinesis. Numbers of embryos analyzed are indicated in the bars. Embryos were obtained from at least three independent pairs. An unpaired Student's *t*-test was used to test for significance. Scale bars: 20  $\mu$ m. Schematics of embryonic development are adapted, with permission, from Kimmel et al. (1995).

scores across all proteins that were detected in both pull downs was 0.71, demonstrating high reliability of the data. Next, the MS scores from both experiments were combined and used for further statistical analysis using the significance analysis of interactome (SAINT) and fold change calculation (Choi et al., 2011; Mellacheruvu et al., 2013) (see detailed description in the Materials and Methods). This resulted in the identification of 88 proteins as putative binding partners of Cfap53 (Table S2). Network and GO analysis enabled us to group these proteins into functional classes (Fig. 3A, Fig. S2).

A large number of proteins from our list are known for their localization in centrosomes and centriolar satellites, such as PCMI, NIN, CEP131, CEP290 and CEP170, which is consistent with the observed colocalization of Cfap53 and PCMI (Balczon et al., 1994; Kim et al., 2008; Kubo et al., 1999; Kubo and Tsukita, 2003; Quarantotti et al., 2019; Silva et al., 2016; Staples et al., 2012; Stowe et al., 2012). PCMI acts as a scaffold for centriolar satellite assembly and facilitates centrosomal protein trafficking (Balczon et al., 1994; Kubo et al., 1999; Kubo and Tsukita, 2003). We therefore compared our protein list with a published list of 211

**Table 2. EdU incorporation**

EdU incubation period	Stage at fixation	EdU incorporation	Unfertilized eggs	Wild type ♀ × wild type ♂*	<i>cfap53</i> <sup>-/-</sup> ♀ × <i>cfap53</i> <sup>-/-</sup> ♂*	Wild type ♀ × <i>cfap53</i> <sup>-/-</sup> ♂*	<i>cfap53</i> <sup>-/-</sup> ♀ × wild type ♂*
A 0-60 mpf	Two cell	+	n.a.	23 (100)	4 (57)	6 (55)	6 (67)
		-	n.a.	0 (0)	3 (43)	5 (45)	3 (33)
		Total	n.a.	23	7	11	9
	One cell	+	0 (0)	3 (20)	26 (47)	14 (88)	18 (55)
		-	23 (100)	12 (80)	29 (53)	2 (12)	15 (45)
		Total	23	15	55	16	33
B 45-105 mpf	Thirty-two cell	+	n.a.	40 (77)	26 (76)	n.d.	n.d.
		-	n.a.	12 (23)	8 (24)	n.d.	n.d.
		Total	n.a.	52	34	n.d.	n.d.
	One cell	+	0 (0)	2 (11)	22 (50)	n.d.	n.d.
		-	26 (100)	16 (89)	22 (50)	n.d.	n.d.
		Total	26	18	44	n.d.	n.d.

Numbers in parentheses are percentages.

n.a., not applicable; n.d., not determined.

\*Results from at least two independent pairs.



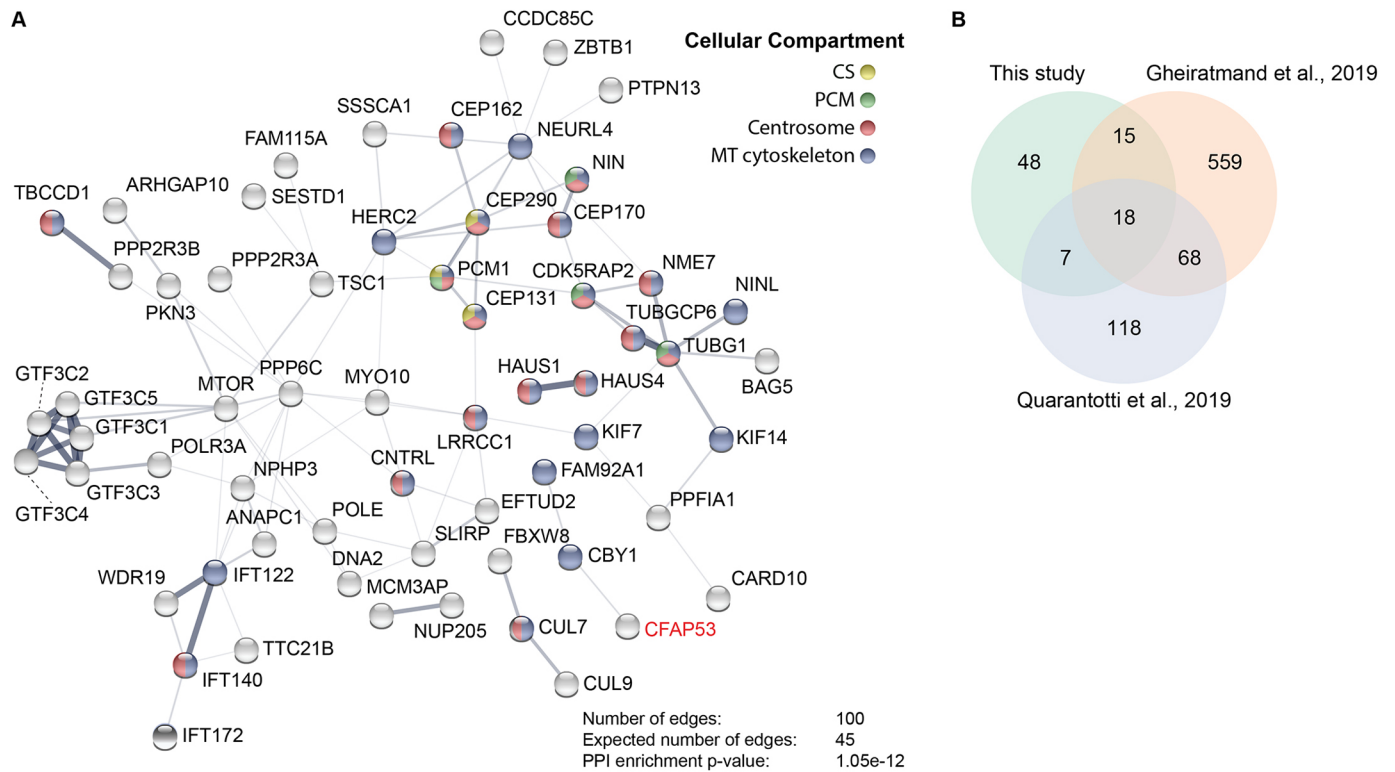


**Fig. 3. Cfp53 interacts with centrosomal, centriolar satellite and microtubule-associated proteins.** (A) Network analysis using String-DB (Szklarczyk et al., 2015) from proteins identified by MS analysis after streptavidin-based purification using CFAP53 as bait. Only high-confidence hits from the MS dataset were used, which were obtained via stringent filtering steps on raw data (see Materials and Methods). Proteins shown are those with a significantly higher number of edges (representing protein-protein associations) than that expected stochastically. The thickness of the lines between the nodes does not represent strength or specificity of a given interaction, but represents the approximate confidence on a scale from zero to one of a found association being true, given the available evidence. Node colors represent cellular compartment of the indicated protein. (B) Venn diagram showing number of proteins identified in this study by bioGFP-Cfp53 pull-down with MS analysis overlapping with the centriolar satellite proteins that were identified by Gheiratmand et al. (2019) and Quarantotti et al. (2019).

satellite proteins resulting from an affinity purification of satellites using PCM1 as bait (Gheiratmand et al., 2019; Quarantotti et al., 2019). We indeed observed a significant overlap with these interactomes, as 25 out of 88 proteins (28%,  $P=1.8 \times 10^{-22}$ ) that were enriched in the bioGFP-Cfp53 pull down were also present in the PCM1 affinity purification (Fig. 3B). In addition, a proximity-dependent biotin identification approach with 22 satellite proteins, including Cfp53, identified an interactome of 660 proteins (Gheiratmand et al., 2019). Comparison with the Cfp53 interactome revealed that 33 out of 88 proteins (37%,  $P=6.4 \times 10^{-18}$ ) overlapped with the centrosomal satellite proteome (Fig. 3B).

Another prominent group of proteins copurifying with Cfp53 are the  $\gamma$ TuRC components  $\gamma$ -tubulin (TUBG1) and GPC6, as well as proteins that interact with  $\gamma$ TuRC, such as CDK5RAP2 and the kinase NME7 (Choi et al., 2010; Liu et al., 2014; Murphy et al., 2001). Moreover, the MS data contained components of HAUS complex (HAUS1 and HAUS4), which localizes to spindles and centrosomes, and controls branching microtubule nucleation (Goshima et al., 2008; Lawo et al., 2009). Together, these data show that Cfp53 can interact with centrosomal and centriolar satellite proteins, as well as proteins with known functions in microtubule nucleation.

### Cfp53 localizes to MTOC during embryonic development

As Cfp53 localization in zebrafish embryos had not been determined, we generated a *Tg(ubi:GFP-Cfp53)* line, in which a GFP-Cfp53 fusion protein is expressed ubiquitously. To test

whether the GFP-Cfp53 protein is functional, the *Tg(ubi:GFP-Cfp53)* was crossed into the *cfap53<sup>hu1047</sup>* line. We first incrossed *Tg(ubi:GFP-Cfp53)/cfap53<sup>+/-</sup>* fish and analyzed their progeny for laterality defects, as we previously described laterality defects in *cfap53<sup>-/-</sup>* embryos (Noël et al., 2016). We found that the laterality defect was rescued in *cfap53<sup>-/-</sup>* embryos expressing the GFP-Cfp53 fusion protein (Fig. S3). Next, we crossed adult *cfap53<sup>-/-</sup>* fish that carried the *Tg(ubi:GFP-Cfp53)*, and their progeny were scored for GFP-Cfp53 expression and embryonic development. Importantly, GFP-Cfp53 was also able to rescue the maternal *cfap53<sup>-/-</sup>* phenotype, as the percentage of arrested embryos in *MPcfap53<sup>-/-</sup>* embryos dropped from 67% to 20% when maternal GFP-Cfp53 was present (Fig. S3). From these results, we concluded that GFP-Cfp53 is a functional protein and therefore could be used to determine the subcellular localization of Cfp53. We investigated the subcellular localization of GFP-Cfp53 in embryos starting at 10 mpf up to 4 hpf and compared it with  $\gamma$ -tubulin localization as a marker for the MTOC (Lindeman and Pelegri, 2012; Rathbun et al., 2020; Yabe et al., 2007). During the first 15 min of development, we observed a weak GFP-Cfp53 signal equally distributed throughout the cytoplasm while some  $\gamma$ -tubulin was localized around the male pronucleus (Fig. 4A,B). At 30 mpf, when the first mitosis of the zygote has started, we observed accumulation of GFP-Cfp53 on either side of the metaphase plate containing the aligned chromosomes. At this stage, we observed for the first time a colocalization of GFP-Cfp53 with  $\gamma$ -tubulin (Fig. 4C). As embryo development proceeds with a new cell

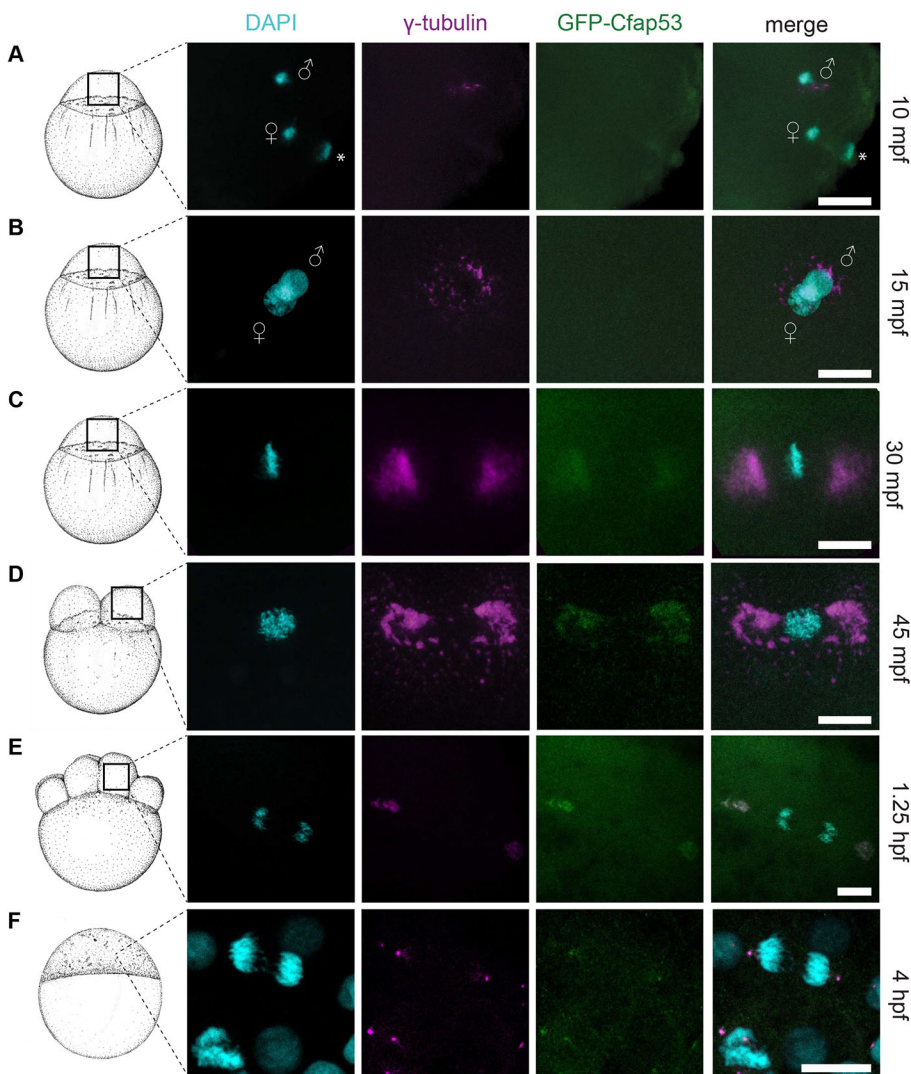


**Fig. 4. GFP-Cfap53 localization during cleavage stages.** (A-F) Maximal projections of confocal stacks from Tg(*ubi:GFP-cfap53*) embryos immunolabelled for GFP,  $\gamma$ -tubulin and DAPI from 30 mpf until 4 hpf. (A) At 10 mpf, male and female pronuclei and the female polar body are visible. Some  $\gamma$ -tubulin foci around the male pronucleus can be observed, while GFP-Cfap53 has a diffuse localization (A,  $n=7$ ). (B) At 15 mpf, both pronuclei are almost fused and some  $\gamma$ -tubulin can be observed around the nuclei, while GFP-Cfap53 localization is still diffuse (B,  $n=7$ ). (C) At 30 mpf, chromosomes have aligned along the metaphase plate and strong  $\gamma$ -tubulin staining can be observed on either side of it. At this moment, GFP-Cfap53 also starts to localize to both sides of the metaphase plate, where it colocalizes with  $\gamma$ -tubulin (C,  $n=12$ ). (D) At 45 mpf, the first cell division has completed and one of the two nuclei is shown. Both GFP-Cfap53 and  $\gamma$ -tubulin are visible in broad domains on both sides of the nucleus during prophase (D,  $n=8$ ). (E) Single cell of an eight-cell stage blastula with segregating chromosomes during telophase of mitosis. GFP-Cfap53 and  $\gamma$ -tubulin colocalize in a more condensed region at both sites of the division plane (E,  $n=7$ ). (F) Blastula cell in telophase during mitosis at the sphere stage (4 hpf). GFP-Cfap53 and  $\gamma$ -tubulin colocalize to a confined region on both sides of the division plane (F,  $n=1$ ). Asterisks indicate polar bodies. Gender symbols indicate male or female pronucleus. Scale bars: 20  $\mu$ m. Schematics of embryonic development are adapted, with permission, from Kimmel et al. (1995).

division every 15 min, both GFP-Cfap53 and  $\gamma$ -tubulin localization became more confined to two structures on either side of the aligned or segregating chromosomes (Fig. 4E,F). Together, these results indicate that, in the egg, GFP-Cfap53 is initially diffusely localized throughout the cytoplasm and that after pronuclear fusion both Cfap53 and  $\gamma$ -tubulin accumulate to form large MTOCs consisting of multiple protein foci. As we observed that paternal Cfap53 facilitates the initiation of the first cell division, we investigated GFP-Cfap53 localization in sperm cells. We observed that the GFP-Cfap53 localizes near the sperm DNA in two domains. The first domain is around the centrioles marked by centrin and the second domain is in a single spot of unknown origin near the centrioles (Fig. S4).

#### Cfap53 facilitates the formation of the MTOC after fertilization

To confirm that GFP-Cfap53 localizes to the MTOC in the zebrafish embryo, we co-stained GFP-Cfap53-expressing embryos with antibodies that recognize centrin. Indeed, we observed colocalization of GFP-Cfap53 with centrin (Fig. 5A-C).

Based on the Cfap53 pull down results and its localization, we examined a possible role of Cfap53 in the formation of the MTOC. As the MS data revealed a possible interaction between Cfap53 with PCM1 and  $\gamma$ -tubulin, we investigated the localization of these and

other centrosomal proteins in wild-type and *MPcfap53*<sup>-/-</sup> embryos. In wild-type embryos,  $\gamma$ -tubulin, PCM1 and centrin were localized in the large MTOC structures typical for early cleavage stage zebrafish embryos (Fig. 5D-F) (Dekens et al., 2003; Lindeman and Pelegri, 2012; Rathbun et al., 2020). In arrested *MPcfap53*<sup>-/-</sup> embryos,  $\gamma$ -tubulin signal was present, albeit at reduced levels, and it formed granule-like foci scattered throughout the cytoplasm (Fig. 5G). The mislocalization of  $\gamma$ -tubulin observed in *MPcfap53*<sup>-/-</sup> embryos was rescued by expression of GFP-Cfap53, resulting in normal chromosome segregation (Fig. S5). In addition, PCM1 and centrin signals were diffuse and no longer accumulated in MTOC structures in arrested *MPcfap53*<sup>-/-</sup> embryos (Fig. 5H,I). In developing *MPcfap53*<sup>-/-</sup> embryos, we observed that  $\gamma$ -tubulin, PCM1 and centrin accumulated at the MTOCs with slight variations in their patterns (Fig. 5J-L), which may be due to natural variation observed among embryos.

Failure in MTOC formation results in a disorganized microtubule network and cell cycle arrest, as proper bipolar spindles cannot be formed (Minshull et al., 1994). To test whether the observed arrest in the first cell cycle of *MPcfap53*<sup>-/-</sup> embryos could be due to defective bipolar spindle formation, we used the Tg(*XIEefl1:dclk2a-GFP*) line, which labels microtubules *in vivo*. As the Dclk2a-GFP fusion protein is maternally provided, we used it to visualize the microtubule network during the first cell division. In



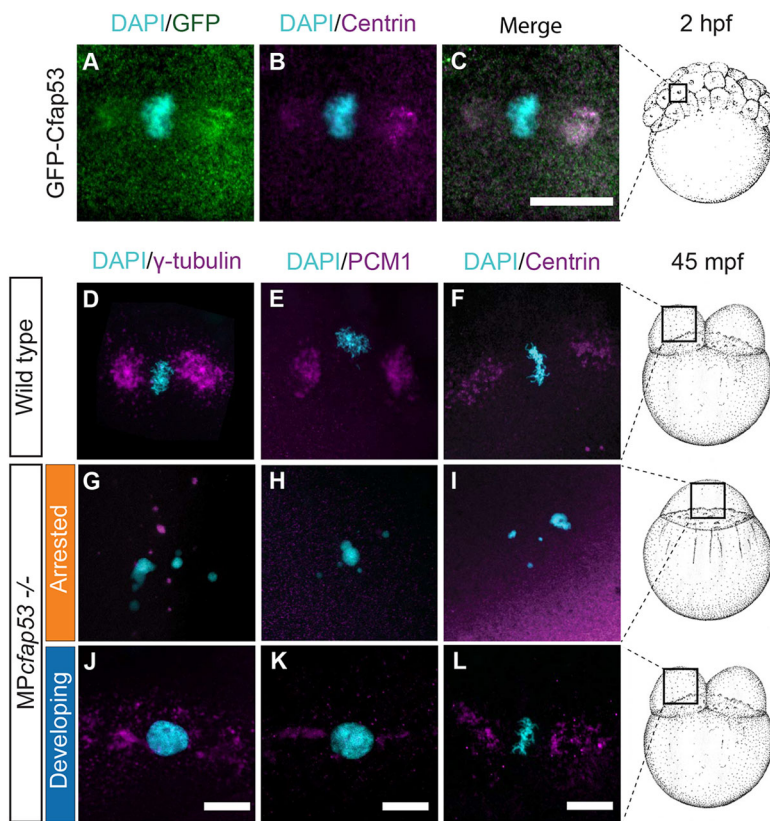


**Fig. 5. Cfap53 is important for the localization of centrosomal components and centriolar satellites at the MTOC.** (A-C,  $n=9$ ) Maximal projections of confocal stacks from fixed Tg(ubi:*GFP-cfap53*) transgenic embryos immunolabeled for centrin at 2 hpf shows strong colocalization of GFP-Cfap53 with centrin during metaphase. (D-L) Maximal projections of confocal stacks from fixed wild-type or *MPcfap53*<sup>-/-</sup> embryos at 45 mpf immunolabeled for centrosomal components.  $\gamma$ -tubulin (D;  $n=8$ ; G,  $n=15$ ; J,  $n=3$ ), PCM1 (E,  $n=7$ ; H,  $n=15$ ; K,  $n=3$ ) and centrin (F,  $n=5$ ; I,  $n=8$ ; L,  $n=14$ ) in wild-type embryos (D-F), *MPcfap53*<sup>-/-</sup> non-developing embryos (G-I) or *MPcfap53*<sup>-/-</sup> developing embryos (J-L) at 45 mpf fixed. Scale bars: 20  $\mu$ m. Schematics of embryonic development are adapted, with permission, from Kimmel et al. (1995).

developing *MPcfap53* embryos, we observed microtubule bundles nucleating from the MTOC to form astral microtubules and a symmetric bipolar spindle (Fig. 6A). However, in *MPcfap53*<sup>-/-</sup> arrested embryos the bipolar spindle was not formed; instead, we observed that microtubule bundles still nucleate but in a disorganized fashion originating from the chromosomes (Fig. 6B), which explains their cell cycle arrest. Taken together, these results indicate that Cfap53 facilitates MTOC formation and therefore the assembly of the mitotic spindle.

#### The microtubule network is important for the zygotic MTOC

When analyzing the Dclk2a-GFP and  $\gamma$ -tubulin colocalization more closely, we noticed that  $\gamma$ -tubulin forms foci varying in size at apparent microtubule ends or dispersed along microtubules. The Dclk2a-GFP and  $\gamma$ -tubulin did not appear to colocalize (Fig. 7A,B), which was confirmed by a very low Pearson's coefficient of 0.0997

for Dclk2a-GFP and  $\gamma$ -tubulin colocalization (Fig. 7B). This observation suggests that at this stage  $\gamma$ -tubulin is associated with the microtubules, similar to what has been shown for PCM1 (Kubo and Tsukita, 2003). Therefore, we investigated whether microtubules are required for  $\gamma$ -tubulin localization at the MTOC. We treated wild-type embryos directly after their fertilization with nocodazole or taxol to either depolymerize or stabilize microtubules, respectively (Fig. 7C). Although taxol treatment arrested the embryos at the metaphase stage during the first mitosis, there was no strong effect on  $\gamma$ -tubulin localization (Fig. 7D). Interestingly, embryos treated with nocodazole showed dispersed cytoplasmic granules of  $\gamma$ -tubulin, similar to those seen in *MPcfap53*<sup>-/-</sup> embryos (compare Fig. 7D with Figs 5D and 6B). We therefore conclude that, in the zebrafish embryo, a functional microtubule network is required for the localization of  $\gamma$ -tubulin at the MTOC.

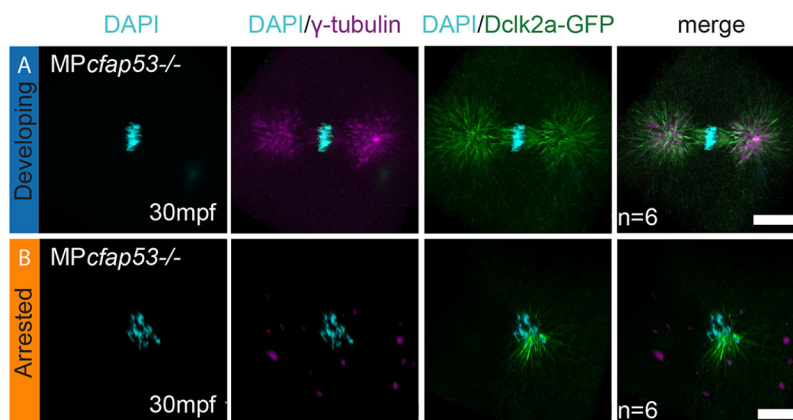


**Fig. 6. Cfap53 facilitates assembly of the zygotic spindle.**

(A,B) Maximal projections of confocal stacks on Tg(*XIEef1a1:dclk2a-GFP*)/*MPcfap53*<sup>-/-</sup> embryos at 30 mpf and immunolabeled for GFP,  $\gamma$ -tubulin and DAPI. While six embryos formed centrosomes and a normal mitotic spindle during the first zygotic cell division (A,  $n=6$ ), six embryos failed to assemble the centrosomes and the mitotic spindle (B,  $n=6$ ). Instead, microtubule originating from the chromosomes is observed in these embryos. Scale bars: 20  $\mu$ m.



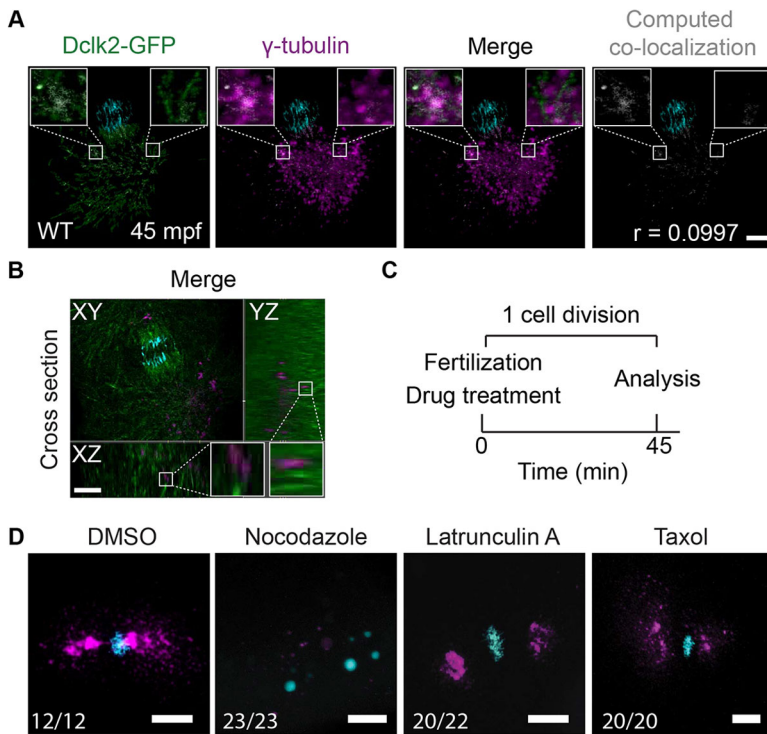


**Fig. 7. Microtubule-dependent  $\gamma$ -tubulin localization.**

(A,B) Maximal projections of confocal stacks from a *Tg(Xla.Eef1a1:Dclk2a-GFP)* embryo immunolabeled for DAPI (in cyan), Dclk2a-GFP (in green) and  $\gamma$ -tubulin (in magenta) at 45 mpf fixed during telophase. Colocalization of  $\gamma$ -tubulin and Dclk2a-GFP is shown in white in the merge. Computation of colocalization gives an average Pearson's coefficient of 0.1, indicating that there is very little colocalization of  $\gamma$ -tubulin and Dclk2a-GFP (A,  $n=5$ ). Scale bar: 100  $\mu$ m. (B) Optical cross-section through 45 mpf embryo immunostained for  $\gamma$ -tubulin and Dclk2a-GFP at the region of one of the centrosomes, which shows that  $\gamma$ -tubulin is localized directly adjacent to the microtubule bundles (B,  $n=5$ ). Scale bar: 100  $\mu$ m. White squares outline the areas shown in more detail. (C) Schematic overview of the drug treatment experiment (C), for which the results are shown in D. (D) Maximal projections of confocal stacks of embryos at 45 mpf immunostained with  $\gamma$ -tubulin (in magenta) and DAPI (in cyan) fixed during telophase. Nocodazole treatment ( $n=23$ ) prevents  $\gamma$ -tubulin accumulation at the MTOC. Latrunculin A ( $n=20$ ) and taxol ( $n=20$ ) treatments have no effect on  $\gamma$ -tubulin localization to the MTOC. Scale bars: 20  $\mu$ m.

## DISCUSSION

After fertilization, a MTOC is assembled from maternal and paternal components. Although this is a crucial step to ensure formation of the sperm aster and the mitotic spindle, which facilitates proper cell division and further development of the embryo, very little is known about its mechanisms and the factors that are involved. In this study, we describe that both maternally and paternally derived Cfap53 protein plays a specific role in the MTOC to form the mitotic spindle, although its role is dispensable for sperm aster assembly, as assessed by normal pronuclear congression.

The cytokinesis defect that we observed in *MPcfap53<sup>-/-</sup>* embryos has an incomplete penetrance (see Table 1). This suggests that the loss of Cfap53 can be compensated for by other mechanisms (see below discussion about diffusion versus active protein transport) or by proteins with a similar function. Recent genetic work in zebrafish has shown that mutations that introduce a premature stop codon in the mRNA, which results in mRNA degradation, can trigger a transcriptional adaptation mechanism (Rossi et al., 2015; Sztal et al., 2018; Zhu et al., 2017). This transcriptional adaptation mechanism causes an upregulation of the expression of related genes and thereby (partially) rescues the phenotype. As the *cfap53<sup>hu10478</sup>* allele is a 7 bp deletion, it results in a frameshift and subsequent introduction of a premature stop codon, which may result in mRNA degradation and activation of the transcriptional adaptation mechanism. mRNA sequencing of oocytes from *cfap53* mutant fish could help to identify the compensating genes.

Our genetic analysis indicates that both maternally and paternally provided Cfap53 protein is important for progression through the first cell division (Fig. 1). Among the very few genes that have been associated with both maternal and paternal functions during the first cell division in *C. elegans* and zebrafish is *zyg-1/sass6* (Yabe et al., 2007; O'Connell et al., 2001). Our finding that paternal Cfap53 is important is consistent with the detection of Cfap53 protein in bovine sperm by mass spectrometry (Firat-Karalar et al., 2014) and

our own results demonstrating the presence of GFP-Cfap53 protein in zebrafish sperm by microscopy (Fig. S4). Thus, although the sperm cell loses most of its PCM and centriolar satellite proteins, Cfap53 is maintained during spermatogenesis. The location of GFP-Cfap53 in sperm is atypical, as most of the protein does not colocalize with the centriole marker. Future research should address the mechanism by which Cfap53 from the sperm contributes to the formation of the mitotic spindle.

After the sperm aster is formed and nuclear congression is completed, GFP-Cfap53 localizes to either side of the fused maternal and paternal pronuclei. This coincides with a clear  $\gamma$ -tubulin accumulation on either side of the nucleus. In earlier stages, we observed only a diffuse GFP-Cfap53 signal, which either indicates a lack of specific localization or a lag in the translation of GFP-Cfap53 protein after fertilization. Lack of Cfap53 accumulation at the sperm aster is consistent with unaffected nuclear congression in *MPcfap53<sup>-/-</sup>* embryos. This is very different from the role of lymphoid-restricted membrane protein (Lrmp), a maternally provided protein required for nuclear congression (Dekens et al., 2003; Lindeman and Pelegri, 2012). The different roles of Cfap53 in the MTOCs forming the sperm aster and the mitotic spindle may be related their difference in composition and size. We and others have observed that PCM1, centrin and  $\gamma$ -tubulin form cytoplasmic accumulations that appear as a large clouds on either side of the nucleus during the first cell divisions of the zebrafish embryo (Dekens et al., 2003; Lindeman and Pelegri, 2012; Rathbun et al., 2020; Stowe et al., 2012). Large MTOCs have also been observed in one-cell stage *Xenopus* embryos and embryos from marine invertebrates (Mitchison, et al., 2012). Why these structures that function as MTOCs are so large at the one-cell stage and become smaller during subsequent cell divisions is not clear, but may be related to the large size of the embryo (see also below). In *C. elegans* embryos, the MTOC does indeed scale with cell size, which is regulated by limited maternal protein pools (Decker et al., 2011). PCM1-, centrin- and  $\gamma$ -tubulin-containing structures depend on Cfap53, as these were not formed in *MPcfap53* embryos.

The biochemical function of Cfp53 is currently unclear. It has three predicted coiled-coil domains, which are low-complexity structures that facilitate protein-protein interactions and are found in numerous centriolar satellite proteins (Gheiratmand et al., 2019; Mason and Arndt, 2004; Quarantotti et al., 2019). It is possible that, similar to the coiled-coil proteins SPD-5, which is a *C. elegans* centrosome component, CFAP53 facilitates MTOC formation by passive liquid-liquid phase separation (Woodruff, 2018; Woodruff et al., 2017).

What could be the mechanism by which Cfp53 recruits  $\gamma$ -tubulin and other components towards the MTOC after fertilization? In general, protein targeting to the MTOC is regulated by two different pathways: (1) active microtubule-based transport using centriolar satellites; and (2) concentration of proteins to the MTOC via passive diffusion (Conkar et al., 2019; Gillingham and Munro, 2000; Hori and Toda, 2017; Khodjakov and Rieder, 1999; Young et al., 2000; Zimmerman and Doxsey, 2000). For a subset of centrosomal proteins, passive diffusion is sufficient in somatic cells, which includes  $\gamma$ -tubulin (Khodjakov and Rieder, 1999). However, passive diffusion of  $\gamma$ -tubulin alone may not be sufficient, as zebrafish embryos have a much larger volumes during the first cell divisions compared with average somatic cells (1000 times larger in case of the zebrafish). This can be overcome by active directional microtubule- and motor-dependent transport. Several studies have shown that recruitment of  $\gamma$ -tubulin towards the centrosome in somatic cells is facilitated by active transport that is dependent on the microtubule network (Quintyne et al., 1999; Schnackenberg et al., 1998; Stearns and Kirschner, 1994; Young et al., 2000). Our observation that  $\gamma$ -tubulin-positive clusters align along microtubules (Fig. 7A,B) and our finding that nocodazole treatment of wild-type zebrafish embryos directly after fertilization inhibits MTOC localization of  $\gamma$ -tubulin (Fig. 7C) are consistent with microtubule dependency of  $\gamma$ -tubulin recruitment.

How is Cfp53 facilitating the active localization of  $\gamma$ -tubulin at the MTOC? Based on its localization in somatic cells, CFAP53 was classified as a centriolar satellite protein (Silva et al., 2016). Both our MS analysis in somatic cells and the widespread granular localization of GFP-Cfp53 in two-cell stage zebrafish embryos, which resembles localization of the satellite marker PCM1, is consistent with localization of Cfp53 in centriolar satellites (Figs 3 and 4D, Table S2). Centriolar satellites are membraneless granules containing proteins that associate and move along microtubules in a dynein-dependent manner to deliver proteins to the centrosome (Dammermann and Merdes, 2002; Kubo et al., 1999). We find that  $\gamma$ -tubulin is highly represented in our GFP-Cfp53 MS analysis, and we observed the simultaneous accumulation and strong colocalization of GFP-Cfp53 with  $\gamma$ -tubulin at the two-cell stage (Figs 3A and 4D, Table S2), which would suggest a direct role for Cfp53 in  $\gamma$ -tubulin localization to the MTOCs. Alternatively, Cfp53 has a more indirect role in facilitating  $\gamma$ -tubulin localization to the MTOCs. We found NME7 and CDK5RAP2 in our MS data, which are both part of the  $\gamma$ -tubulin ring complex and are recruited in a dynein-dependent manner (Fig. 3A, Table S2) (Choi et al., 2010; Hutchins et al., 2010; Jia et al., 2013; Liu et al., 2014). Defects in centriolar satellites from MPc $cfap53$  mutant embryos may therefore result in the absence of other proteins that are required to recruit  $\gamma$ -tubulin. Importantly, the loss of centriolar satellites in somatic cells, by PCM1 depletion, has little effect on the integrity of the centrosome (Gheiratmand et al., 2019), indicating a clear difference in the role of centriolar satellites in fertilized eggs and somatic cells.

In conclusion, we discovered a novel function for paternally and maternally derived Cfp53 in the formation of the mitotic spindle in

zebrafish embryos. Although Cfp53 protein is dispensable for the function of the sperm aster during nuclear congression, it aids the formation of the MTOC from which the mitotic spindle is formed.

## MATERIALS AND METHODS

### Zebrafish genetics and strains

The following fish lines were used in this study: Tupfel Longfin (TL), *cfap53*<sup>hu10478</sup> (Noël et al., 2016), Tg(*h2afz:GFP*) (Pauls et al., 2001), Tg(*Xla.Eef1a1:dclk2a-GFP*) (Tran et al., 2012) and Tg(*ubi:GFP-cfp53*). Fish were maintained at 27.5°C in a 14/10 h light/dark cycle, according to standard laboratory conditions (Aleström et al., 2020). Embryos were collected and staged according to Kimmel et al. (1995). Animal experiments were approved by the Animal Experimentation Committee (DEC) of the Royal Netherlands Academy of Arts and Sciences (KNAW).

### Plasmid construction and transgenesis

The following plasmids were generated in this study: bioEGFP-CFAP53, CFAP53-EGFPbio and GFP-Cfp53 containing tol2 sites. Human *CFAP53* coding sequence (CDS) was obtained by performing PCR on a PCS2 construct containing human *CFAP53* cDNA and cloned into the pbioEGFP-C1 and pbioEGFP-N1 constructs using the Gibson cloning system (Noël et al., 2016), which are modified pEGFP-C1 and pEGFP-N1, respectively, in which a linker encoding the sequence MASGLNDIFEAQKIEWHEGGG (which is the substrate of biotin ligase BirA) was inserted in front of or behind the eGFP-encoding sequence.

The zebrafish *GFP-cfp53* construct was obtained from Narasimhan et al. (2015) and cloned into the pME-MCS followed by recombination with p5E'-Ubi (Mosimann et al., 2011), p3E-polyA and pDestTol2pA7 using the multisite gateway cloning strategy (Kwan et al., 2007). The plasmid DNA was injected at 30 ng/ $\mu$ l in the presence of 25 ng Tol2 mRNA for genomic integration and to generate Tg(*ubi:GFP-cfp53*). At 3 dpf, healthy embryos displaying robust GFP fluorescence in the cilia were selected and grown to adulthood. Subsequently, founder fish were identified by outcrossing and their progeny grown to adulthood to establish the transgenic line.

### EdU labeling

For EdU detection, the Click-iT EdU Imaging Kit with Alexa Fluor 488 (Thermo Fisher) was used. The stock solutions were prepared according to the provided protocol included in the kit (5 mg/ml EdU stock solution). For EdU incubation, a fresh working solution of 10% DMSO/50  $\mu$ g/ml EdU diluted in E3 water was prepared in 1.5 ml Eppendorf tubes containing a total volume of 1 ml. Fish were set-up in pairs and eggs were collected either directly after laying or after 45 mpf. After collection the eggs were transferred into the EdU solution using a transfer pipet and incubated for 30 min on ice in the dark. The embryos were then transferred to a 28°C incubator to incubate for 30 min. After incubation, the embryos were transferred into fresh E3 water for a short rinse and directly fixed after with microtubule fix (3.7% formaldehyde, 0.25% glutaraldehyde, 5 mM EGTA and 0.3% Triton X-100) for 2 h at room temperature as described below in the 'Fixation and antibody labeling' section. Detection of EdU was performed according to the protocol described in the Click-iT EdU Imaging Kit. The imaging of the EdU detection was performed as described in the 'Imaging' section below.

### Cell culture

Human embryonic kidney 239T (HEK293T) and HeLa (Kyoto) cell lines were cultured in medium that consisted of 45% DMEM, 45% Ham's F10 and 10% fetal calf serum supplemented with penicillin and streptomycin. The cell lines were routinely checked for mycoplasma contamination using LT07-518 Mycoalert assay (Lonza). For the immunolabeling experiment, HeLa cells were transfected with plasmids using FuGENE 6 (Promega). For streptavidin pull-down assays from HEK293T cells, plasmids were transfected using polyethylenimine (Polysciences).

### Streptavidin pull-down assays

Streptavidin pull-down assays were performed from HEK293T cell lysates by co-expressing biotin ligase BirA with GFP-tagged constructs containing

a biotinylation site (bioGFP-CFAP53 and CFAP53-GFPbio) and only expressing biotin ligase BirA as a negative control. Constructs were transfected together into HEK293 cells using polyethylenimine (PEI, Polysciences) with a 24 h incubation time for protein expression. M-280 Streptavidin Dynabeads (Invitrogen) were blocked in a buffer containing 20 mM Tris (pH 7.5), 20% glycerol, 150 mM NaCl and 10 µg chicken egg albumin followed by three washes with wash buffer containing 20 mM Tris (pH 7.5), 150 mM NaCl and 0.1% Triton X-100. HEK293T cells were collected in ice-cold PBS followed by lysis on ice in a buffer containing 20 mM Tris (pH 7.5), 150 mM NaCl, 1 mM MgCl<sub>2</sub>, 1% Triton X-100 and complete protease inhibitor cocktail (Roche). To separate cell debris, the lysates were cleared by centrifugation at 16,000 *g* at 4°C for 20 min. Cell lysates were incubated with pre-blocked streptavidin beads for 120 min at 4°C followed by five washes with a buffer containing 20 mM Tris (pH 7.5), 150 mM NaCl and 0.1% Triton X-100 (Hooikaas et al., 2019).

### Mass spectrometry analysis

Beads were re-suspended in 20 µl of Laemmli Sample buffer (BioRad) and supernatants were loaded on a 4–12% gradient Criterion XT Bis-Tris precast gel (BioRad). The gel was fixed with 40% methanol/10% acetic acid and then stained for 1 h using colloidal Coomassie dye G-250 (Gel Code Blue Stain Reagent, ThermoFisher Scientific). After in-gel digestion (Noordstra et al., 2016), all samples were analyzed on a Orbitrap Q-Exactive HF mass spectrometer (ThermoFisher Scientific) coupled to an Agilent 1290 Infinity LC. Peptides were loaded onto a trap column (Reprosil C18, 3 µm, 2 cm×100 µm; Dr. Maisch) with solvent A (0.1% formic acid in water) at a maximum pressure of 800 bar and chromatographically separated over the analytical column (Zorbax SB-C18, 1.8 µm, 40 cm×50 µm; Agilent) using 90 min linear gradient from 7–30% solvent B (0.1% formic acid in acetonitrile) at a flow rate of 150 nl/min. The mass spectrometer was used in a data-dependent mode, which automatically switched between MS and MS/MS. After a survey scan from 350–1500 *m/z* the 12 most abundant peptides were subjected to HCD fragmentation. For data analysis, raw files were processed using Proteome Discoverer 1.4 (Thermo Scientific). Database searches were performed using Mascot as search engine on the Human Uniprot database. Carbamidomethylation of cysteines was set as a fixed modification and oxidation of methionine was set as a variable modification. Trypsin was set as cleavage specificity, allowing a maximum of two missed cleavages. Data filtering was performed using percolator, resulting in 1% false discovery rate (FDR). Additional filters were search engine rank 1 and mascot ion score >20. To retrieve significant putative binding partners of CFAP53 additional analyses on the raw MS data were performed using contaminant repository for affinity purification (the CRAPome) implementing fold change scoring (FC) scoring and probabilistic scoring using SAINT. The FC is calculated based on the ratio of average normalized spectral counts in bait purifications to negative controls. SAINT uses statistical modeling which provides a probability of true interaction (Choi et al., 2011; Mellacheruvu et al., 2013). The FC scoring is subdivided into a FCA (primary score based on BirA negative control pull down) and FCB (secondary score based on existing GFP negative control). The FCA and FCB cut-offs were set to seven and three, respectively. The SAINT probability cut-off was set to 0.95.

### Drug treatments

To destabilize or stabilize the microtubule network 4 µg/ml nocodazole (1 mg/ml stock dissolved in DMSO) and 10 µM taxol (1 mM stock dissolved in DMSO) were used, respectively. To inhibit actin, 25 µM latrunculin A (5 mM stock dissolved in DMSO) was used. Embryos from the same fish were collected directly after fertilization and treated with the drug or DMSO control for 45 min, corresponding to the duration of the first cell division. Embryos were subsequently washed in E3 medium prior to fixation in microtubule fix as below and stained for  $\gamma$ -tubulin.

### mRNA transcription and injection

The PCS2-GFP-Cfap53 construct was linearized with NotI and used as template for transcription of capped mRNA (mMessage SP6 kit, Ambion, AM1340). mRNA was purified using lithium chloride precipitation and

re-suspension in nuclease-free water. mRNA was injected into the yolk of one-cell stage embryos in a volume of 1 nl at a concentration of 100 ng/µl.

### Fixation and antibody labeling

For immunolabeling, HeLa cells were fixed in –20°C methanol for 10 min. Cells were then permeabilized with 0.15% Triton X-100 in PBS for 2 min; subsequent wash steps were performed in PBS supplemented with 0.05% Tween-20. Epitope blocking and antibody labeling steps were performed in PBS supplemented with 0.05% Tween-20 and 1% BSA. Before mounting in Vectashield mounting medium (Vector Laboratories), slides were washed with 70% and 100% ethanol and air-dried (Hooikaas et al., 2019).

Zebrafish embryos were collected at the appropriate stages during development and fixed for 2 h at room temperature in microtubule fix (3.7% formaldehyde, 0.25% glutaraldehyde, 5 mM EGTA and 0.3% Triton X-100) at the indicated stages. After fixation, embryos were washed three times with PBS and Triton X-100 (0.3% PBST) and manually dechorionated. Embryos were dehydrated in methanol overnight at –20°C and rehydrated in a methanol:PBS series. Before labeling, embryos were treated with 0.5 mg/ml sodium borohydride for 30 min at room temperature to inactivate remaining glutaraldehyde. Subsequently, embryos were washed in PBST and yolks were manually separated from the cells using forceps. Embryos were blocked in 0.3% PBST, 2% BSA and 10% sheep serum for 1 h at room temperature. Commercial antibodies used were as followed: anti-PCM1 (Sigma, rabbit polyclonal, 1:200), anti- $\gamma$ -tubulin (Sigma, mouse monoclonal GTU-88, 1:500), anti-centrin (Millipore, monoclonal mouse IgG2a 1:200) and anti-GFP (Aves, chicken, 1:500). All primary antibodies were incubated overnight at 4°C. Primary antibodies were detected using Alexa Fluor 488 (Invitrogen, goat anti-mouse), Alexa Fluor 488 (Invitrogen, goat anti-chicken, IgG1) and Alexa Fluor 555 (Invitrogen, goat anti-mouse, IgG1). Nuclei were shown by DAPI (4',6-diamidino-2-phenylindole) staining.

### Imaging

Fixed embryos were embedded in 0.25% agarose to be mounted on a glass bottomed dish. Subsequently, embryos were imaged using a Leica SP5 Multi Photon setup (Leica Microsystems) using a 25× water and 63× glycerol objective followed by a z-stack maximum projection (step size 1 µm).

For generation of time lapse videos, live embryos were embedded in 0.25% agarose to be mounted on a glass bottom dish. Subsequently, embryos were imaged live using a temperature controlled AF7000 Widefield Fluorescence Microscope setup (Leica Microsystems) using a 10× dry objective maintaining the temperature at a constant 28°C. The interval between images was set to 2 min. Computation of colocalization was performed using the 3D colocalization tool in Bitplane Imaris software (V9.3.1).

### Sperm motility evaluation by computer-assisted sperm analysis (CASA)

Sperm cells were extracted from *cfap53*<sup>–/–</sup> and wild-type males as previously described (Dooley et al., 2013). Directly after collection, sperm cells were transferred into 50 µl of buffered sperm-motility inhibiting solution (BSMIS) on ice. Motility was assessed on the computer-assisted semen analysis (CASA) system Sperm Vision (version 3.5, Minitüb). The system was operated at room temperature with an automated stage and four-chamber slides of 20 µm depth (Leja). After sperm activation in tap water, a 3.0 µl aliquot was immediately transferred to each chamber. Motility assessments started ~12 s after motility activation. Spermatozoa were examined at 200× magnification by a camera with a resolution of 648×484 pixels (Pulnix TM-6760CL, JAI A/S). The Sperm Vision software analyzed 15 successive fields in the central part of the chamber at a frame rate of 60 Hz per field. Acquisition time for each field was 0.5 s. The surface area for sperm head detection was set at 4 to 80 µm<sup>2</sup>. The setup ensured that, in the majority of samples (11 out of 14), more than 1000 spermatozoa could be analyzed (mean of 1897 sperm).

Semen samples were assessed for the percentage of motile (total motility) and progressively motile spermatozoa (progressive motility). The following



motility descriptors were recorded for each motile spermatozoon: straight line velocity (VSL), curved line velocity (VCL), average path velocity (VAP), linearity (LIN=VSL/VCL), straightness (STR=VSL/VAP), wobble (WOB=VAP/VCL), average amplitude of lateral head-displacement (ALH) and beat cross frequency (BCF). A spermatozoon was considered to be motile when it met one of the following three definitions: (1) average head orientation change (AOC) higher than 7° and BCF greater than 25 Hz; (2) DSL greater than 3.5 μm, VSL greater than 8 μm/s and DSL greater than 15 μm; or (3) VAP greater than 15 μm/s. Significance between wild-type and mutant spermatozoa was calculated using a paired Student's *t*-test (Table S1).

### Primers

Primers used were as follows: *cfap53* genotyping FW\_*cfap53*, 5'-TGTA-AGGAGAAGGAAGCAGGA; *cfap53* genotyping RV\_*cfap53*, 3'-TCAT-CAATGCCCATCTGGTA; and *cfap53* genotyping in GFP-*cfap53* transgenic background FW\_*cfap53*, GGTGCTGGAGTTCACCAAAG; *cfap53* genotyping in GFP-*cfap53* transgenic background RV\_*cfap53* intron, 3'-ccgctcagacTTTCCCTCT. Uppercase and lowercase letters indicate exons and introns, respectively.

### Acknowledgements

We thank W. Makkinje for technical assistance with generating the GFP-Cfap53 transgenic line and M. Mullins for helpful discussions.

### Competing interests

The authors declare no competing or financial interests.

### Author contributions

Conceptualization: S.W., F.T., A.A., J.B.; Methodology: S.W., F.T., J.B.; Validation: S.W.; Formal analysis: S.W., F.T., B.v.d.V., H.H.H., R.S.; Investigation: S.W., F.T., B.v.d.V., H.H.H., R.S.; Resources: S.W., B.v.d.V., H.H.H., R.S., M.A., B.A.J.R., A.A., J.B.; Data curation: F.T.; Writing - original draft: S.W., J.B.; Writing - review & editing: S.W., F.T., B.v.d.V., H.H.H., R.S., M.A., B.A.J.R., A.A., J.B.; Visualization: S.W., F.T.; Supervision: F.T., A.A., J.B.; Project administration: S.W., J.B.; Funding acquisition: A.A., J.B.

### Funding

This research was part of the Netherlands X-omics Initiative and partially funded by the Nederlandse Organisatie voor Wetenschappelijk Onderzoek (project 184.034.019 and OCENW.GROOT.2019.029). Open Access funding provided by the Hubrecht Institute. Deposited in PMC for immediate release.

### Peer review history

The peer review history is available online at <https://journals.biologists.com/dev/lookup/doi/10.1242/dev.198762.reviewer-comments.pdf>.

### References

- Abrams, E. W., Fuentes, R., Marlow, F. L., Kobayashi, M., Zhang, H., Lu, S., Kapp, L., Joseph, S. R., Kugath, A., Gupta, T. et al. (2020). Molecular genetics of maternally-controlled cell divisions. *PLoS Genet.* **16**, e1008652. doi:10.1371/journal.pgen.1008652
- Aleström, P., D'Angelo, L., Midtlyng, P. J., Schorderet, D. F., Schulte-Merker, S., Sohm, F. and Warner, S. (2020). Zebrafish: Housing and husbandry recommendations. *Lab. Anim.* **54**, 213-224. doi:10.1177/0023677219869037
- Bakkers, J., Verhoeven, M. C. and Abdelilah-Seyfried, S. (2009). Shaping the zebrafish heart: From left-right axis specification to epithelial tissue morphogenesis. *Dev. Biol.* **330**, 213-220. doi:10.1016/j.ydbio.2009.04.011
- Balczon, R., Bao, L. and Zimmer, W. E. (1994). PCM-1, A 228-kD centrosome autoantigen with a distinct cell cycle distribution. *J. Cell Biol.* **124**, 783-793. doi:10.1083/jcb.124.5.783
- Choi, Y.-K., Liu, P., Sze, S. K., Dai, C. and Qi, R. Z. (2010). CDK5RAP2 stimulates microtubule nucleation by the  $\gamma$ -tubulin ring complex. *J. Cell Biol.* **191**, 1089-1095. doi:10.1083/jcb.201007030
- Choi, H., Larsen, B., Lin, Z.-Y., Breikreutz, A., Mellacheruvu, D., Fermin, D., Qin, Z. S., Tyers, M., Gingras, A.-C. and Nesvizhskii, A. I. (2011). SAINT: probabilistic scoring of affinity purification-mass spectrometry data. *Nat. Methods* **8**, 70-73. doi:10.1038/nmeth.1541
- Conkar, D., Bayraktar, H. and Firat-Karalar, E. N. (2019). Centrosomal and ciliary targeting of CCDC66 requires cooperative action of centriolar satellites, microtubules and molecular motors. *Sci. Rep.* **9**, 14250. doi:10.1038/s41598-019-50530-4
- Dammermann, A. and Merdes, A. (2002). Assembly of centrosomal proteins and microtubule organization depends on PCM-1. *J. Cell Biol.* **159**, 255-266. doi:10.1083/jcb.200204023
- Decker, M., Jaensch, S., Pozniakovskiy, A., Zinke, A., O'Connell, K. F., Zachariae, W., Myers, E. and Hyman, A. A. (2011). Limiting amounts of centrosome material set centrosome size in *C. elegans* embryos. *Curr. Biol.* **21**, 1259-1267. doi:10.1016/j.cub.2011.06.002
- Dekens, M. P. S., Pelegri, F. J., Maischein, H.-M. and Nüsslein-Volhard, C. (2003). The maternal-effect gene futile cycle is essential for pronuclear congression and mitotic spindle assembly in the zebrafish zygote. *Development* **130**, 3907-3916. doi:10.1242/dev.00606
- Dooley, C. M., Scahill, C., Fényes, F., Kettleborough, R. N. W., Stemple, D. L. and Busch-Nentwich, E. M. (2013). Multi-allelic phenotyping—a systematic approach for the simultaneous analysis of multiple induced mutations. *Methods* **62**, 197-206. doi:10.1016/j.jmeth.2013.04.013
- Doxsey, S. (2001). Re-evaluating centrosome function. *Nat. Rev. Mol. Cell Biol.* **2**, 688-698. doi:10.1038/35089575
- Félix, M. A., Antony, C., Wright, M. and Maro, B. (1994). Centrosome assembly in vitro: role of gamma-tubulin recruitment in *Xenopus* sperm aster formation. *J. Cell Biol.* **124**, 19-31. doi:10.1083/jcb.124.1.19
- Firat-Karalar, E. N., Sante, J., Elliott, S. and Stearns, T. (2014). Proteomic analysis of mammalian sperm cells identifies new components of the centrosome. *J. Cell Sci.* **127**, 4128-4133. doi:10.1242/jcs.157008
- Gheiratmand, L., Coyaud, E., Gupta, G. D., Laurent, E. M. N., Hasegan, M., Prosser, S. L., Gonçalves, J., Raught, B. and Pelletier, L. (2019). Spatial and proteomic profiling reveals centrosome-independent features of centriolar satellites. *EMBO J.* **38**, e101109. doi:10.15252/embj.2018101109
- Gillingham, A. K. and Munro, S. (2000). The PACT domain, a conserved centrosomal targeting motif in the coiled-coil proteins AKAP450 and pericentrin. *EMBO Rep.* **1**, 524-529. doi:10.1093/embo-reports/kvd105
- Goshima, G., Mayer, M., Zhang, N., Stuurman, N. and Vale, R. D. (2008). Augmin: a protein complex required for centrosome-independent microtubule generation within the spindle. *J. Cell Biol.* **181**, 421-429. doi:10.1083/jcb.200711053
- Gould, R. R. and Borisy, G. G. (1977). The pericentriolar material in Chinese hamster ovary cells nucleates microtubule formation. *J. Cell Biol.* **73**, 601-615. doi:10.1083/jcb.73.3.601
- Gueth-Hallonet, C., Antony, C., Aghion, J., Santa-Maria, A., Lajoie-Mazenc, I., Wright, M. and Maro, B. (1993). gamma-Tubulin is present in acentriolar MTOCs during early mouse development. *J. Cell Sci.* **105**, 157-166. doi:10.1242/jcs.105.1.157
- Hirokawa, N., Tanaka, Y., Okada, Y. and Takeda, S. (2006). Nodal flow and the generation of left-right asymmetry. *Cell* **125**, 33-45. doi:10.1016/j.cell.2006.03.002
- Holy, J. and Schatten, G. (1997). Recruitment of maternal material during assembly of the zygote centrosome in fertilized sea urchin eggs. *Cell Tissue Res.* **289**, 285-297. doi:10.1007/s004410050875
- Hooikaas, P. J., Martin, M., Mühlethaler, T., Kuijntjes, G.-J., Peeters, C. A. E., Katrukha, E. A., Ferrari, L., Stucchi, R., Verhagen, D. G. F., Van Riel, W. E. et al. (2019). MAP7 family proteins regulate kinesin-1 recruitment and activation. *J. Cell Biol.* **218**, 1298-1318. doi:10.1083/jcb.201808065
- Hori, A. and Toda, T. (2017). Regulation of centriolar satellite integrity and its physiology. *Cell. Mol. Life Sci.* **74**, 213-229. doi:10.1007/s00018-016-2315-x
- Huang, D. W., Sherman, B. T. and Lempicki, R. A. (2009). Bioinformatics enrichment tools: paths toward the comprehensive functional analysis of large gene lists. *Nucleic Acids Res.* **37**, 1-13. doi:10.1093/nar/gkn923
- Hutchins, J. R. A., Toyoda, Y., Hegemann, B., Poser, I., Hériché, J.-K., Sykora, M. M., Augsburg, M., Hudecz, O., Buschhorn, B. A., Bulkescher, J. et al. (2010). Systematic analysis of human protein complexes identifies chromosome segregation proteins. *Science* **328**, 593-599. doi:10.1126/science.1181348
- Ide, T., Twan, W. K., Lu, H., Ikawa, Y., Lim, L.-X., Henninger, N., Nishimura, H., Takaoka, K., Narasimhan, V., Yan, X. et al. (2020). CFAP53 regulates mammalian cilia-type motility patterns through differential localization and recruitment of axonemal dynein components. *PLoS Genet.* **16**, e1009232. doi:10.1371/journal.pgen.1009232
- Inoue, D., Stemmer, M., Thumberger, T., Ruppert, T., Bärenz, F., Wittbrodt, J. and Gruss, O. J. (2017). Expression of the novel maternal centrosome assembly factor Wdr8 is required for vertebrate embryonic mitoses. *Nat. Commun.* **8**, 14090. doi:10.1038/ncomms14090
- Jia, Y., Fong, K.-W., Choi, Y.-K., See, S.-S. and Qi, R. Z. (2013). Dynamic recruitment of CDK5RAP2 to centrosomes requires its association with dynein. *PLoS ONE* **8**, e68523. doi:10.1371/journal.pone.0068523
- Khodjakov, A. and Rieder, C. L. (1999). The sudden recruitment of  $\gamma$ -tubulin to the centrosome at the onset of mitosis and its dynamic exchange throughout the cell cycle, do not require microtubules. *J. Cell Biol.* **146**, 585-596. doi:10.1083/jcb.146.3.585
- Kim, J., Krishnaswami, S. R. and Gleeson, J. G. (2008). CEP290 interacts with the centriolar satellite component PCM-1 and is required for Rab8

- localization to the primary cilium. *Hum. Mol. Genet.* **17**, 3796-3805. doi:10.1093/hmg/ddn277
- Kimmel, C. B., Ballard, W. W., Kimmel, S. R., Ullmann, B. and Schilling, T. F.** (1995). Stages of embryonic development of the zebrafish. *Dev. Dyn.* **203**, 253-310. doi:10.1002/aja.1002030302
- Kollman, J. M., Merdes, A., Mourey, L. and Agard, D. A.** (2011). Microtubule nucleation by  $\gamma$ -tubulin complexes. *Nat. Rev. Mol. Cell Biol.* **12**, 709-721. doi:10.1038/nrm3209
- Kubo, A. and Tsukita, S.** (2003). Non-membranous granular organelle consisting of PCM-1: subcellular distribution and cell-cycle-dependent assembly/disassembly. *J. Cell Sci.* **116**, 919-928. doi:10.1242/jcs.00282
- Kubo, A., Sasaki, H., Yuba-Kubo, A., Tsukita, S. and Shiina, N.** (1999). Centriolar satellites: Molecular characterization, ATP-dependent movement toward centrosomes and possible involvement in ciliogenesis. *J. Cell Biol.* **147**, 969-980. doi:10.1083/jcb.147.5.969
- Kwan, K. M., Fujimoto, E., Grabher, C., Mangum, B. D., Hardy, M. E., Campbell, D. S., Parant, J. M., Yost, H. J., Kanki, J. P. and Chien, C.-B.** (2007). The Tol2kit: a multisite gateway-based construction kit for Tol2 transposon transgenesis constructs. *Dev. Dyn.* **236**, 3088-3099. doi:10.1002/dvdy.21343
- Lawo, S., Bashkurov, M., Mullin, M., Ferreria, M. G., Kittler, R., Habermann, B., Tagliaferro, A., Poser, I., Hutchins, J. R. A., Hegemann, B. et al.** (2009). HAUS, the 8-subunit human Augmin complex, regulates centrosome and spindle integrity. *Curr. Biol.* **19**, 816-826. doi:10.1016/j.cub.2009.04.033
- Lindeman, R. E. and Pelegri, F.** (2012). Localized products of futile cycle/ lmp promote centrosome-nucleus attachment in the zebrafish zygote. *Curr. Biol.* **22**, 843-851. doi:10.1016/j.cub.2012.03.058
- Liu, P., Choi, Y.-K. and Qi, R. Z.** (2014). NME7 is a functional component of the  $\gamma$ -tubulin ring complex. *Mol. Biol. Cell* **25**, 2017-2025. doi:10.1091/mbc.e13-06-0339
- Mason, J. M. and Arndt, K. M.** (2004). Coiled Coil Domains: Stability, Specificity, and Biological Implications. *ChemBiochem* **5**, 170-176. doi:10.1002/cbic.200300781
- Mellacheruvu, D., Wright, Z., Couzens, A. L., Lambert, J.-P., St-Denis, N. A., Li, T., Miteva, Y. V., Hauri, S., Sardi, M. E., Low, T. Y. et al.** (2013). The CRAPome: A contaminant repository for affinity purification-mass spectrometry data. *Nat. Methods* **10**, 730-736. doi:10.1038/nmeth.2557
- Minshull, J., Sun, H., Tonks, N. K. and Murray, A. W.** (1994). A MAP kinase-dependent spindle assembly checkpoint in *Xenopus* egg extracts. *Cell* **79**, 475-486. doi:10.1016/0092-8674(94)90256-9
- Mitchison, T., Wühr, M., Nguyen, P., Ishihara, K., Groen, A. and Field, C. M.** (2012). Growth, interaction, and positioning of microtubule asters in extremely large vertebrate embryo cells. *Cytoskeleton* **69**, 738-750. doi:10.1002/cm.21050
- Moritz, M., Zheng, Y., Alberts, B. M. and Oegema, K.** (1998). Recruitment of the  $\gamma$ -tubulin ring complex to *Drosophila* salt-stripped centrosome scaffolds. *J. Cell Biol.* **142**, 775-786. doi:10.1083/jcb.142.3.775
- Mosimann, C., Kaufman, C. K., Li, P., Pugach, E. K., Tamplin, O. J. and Zon, L. I.** (2011). Ubiquitous transgene expression and Cre-based recombination driven by the ubiquitin promoter in zebrafish. *Development* **138**, 169-177. doi:10.1242/dev.059345
- Murphy, S. M., Preble, A. M., Patel, U. K., O'Connell, K. L., Dias, D. P., Moritz, M., Agard, D., Stults, J. T. and Stearns, T.** (2001). GCP5 and GCP6: two new members of the human  $\gamma$ -tubulin complex. *Mol. Biol. Cell* **12**, 3340-3352. doi:10.1091/mbc.12.11.3340
- Narasimhan, V., Hjejri, R., Vij, S., Loges, N. T., Wallmeier, J., Koerner-Rettberg, C., Werner, C., Thamilselvam, S. K., Boey, A., Choksi, S. P. et al.** (2015). Mutations in CCDC11, which encodes a coiled-coil containing ciliary protein, causes situs inversus due to dysmotility of monocilia in the left-right organizer. *Hum. Mutat.* **36**, 307-318. doi:10.1002/humu.22738
- Noël, E. S., Momenah, T. S., Al-Daghir, K., Al-Suwaid, A., Al-Shahrani, S., Jiang, H., Willekers, S., Oostveen, Y. Y., Chocron, S., Postma, A. V. et al.** (2016). A zebrafish loss-of-function model for human CFAP53 mutations reveals its specific role in laterality organ function. *Hum. Mutat.* **37**, 194-200. doi:10.1002/humu.22928
- Noordstra, I., Liu, Q., Nijenhuis, W., Hua, S., Jiang, K., Baars, M., Rimmelzwaal, S., Martin, M., Kapitein, L. C. and Akhmanova, A.** (2016). Control of apico-basal epithelial polarity by the microtubule minus-end-binding protein CAMSAP3 and spectraplakins ACF7. *J. Cell Sci.* **129**, 4278-4288. doi:10.1242/jcs.194878
- O'Connell, K. F., Caron, C., Kopish, K. R., Hurd, D. D., Kempthues, K. J., Li, Y. and White, J. G.** (2001). The *C. elegans* zyg-1 gene encodes a regulator of centrosome duplication with distinct maternal and paternal roles in the embryo. *Cell* **105**, 547-558. doi:10.1016/s0092-8674(01)00338-5
- Odabasi, E., Gul, S., Kavakli, I. H. and Firat-Karalar, E. N.** (2019). Centriolar satellites are required for efficient ciliogenesis and ciliary content regulation. *EMBO Rep.* **20**, e47723. doi:10.15252/embr.201947723
- Pauls, S., Geldmacher-Voss, B. and Campos-Ortega, J. A.** (2001). A zebrafish histone variant H2A. F/Z and a transgenic H2A. F/Z: GFP fusion protein for in vivo studies of embryonic development. *Dev. Genes Evol.* **211**, 603-610. doi:10.1007/s00427-001-0196-x
- Pelegri, F. and Mullins, M.** (2016). Genetic screens for mutations affecting adult traits and parental-effect genes. *Methods Cell Biol.* **135**, 39-87. doi:10.1016/bs.mcb.2016.05.006
- Perles, Z., Cinnamon, Y., Ta-Shma, A., Shaag, A., Einbinder, T., Rein, A. J. J. T. and Elpeleg, O.** (2012). A human laterality disorder associated with recessive CCDC11 mutation. *J. Med. Genet.* **49**, 386-390. doi:10.1136/jmedgenet-2011-100457
- Prosser, S. L. and Pelletier, L.** (2020). Centriolar satellite biogenesis and function in vertebrate cells. *J. Cell Sci.* **133**, jcs239566. doi:10.1242/jcs.239566
- Quarantotti, V., Chen, J. X., Tischer, J., Gonzalez Tejedo, C., Papachristou, E. K., D'Santos, C. S., Kilmartin, J. V., Miller, M. L. and Gergely, F.** (2019). Centriolar satellites are centriolar assemblies of centrosomal proteins. *EMBO J.* **38**, e101082. doi:10.15252/embj.2018101082
- Quintyne, N. J., Gill, S. R., Eckley, D. M., Crego, C. L., Compton, D. A. and Schroer, T. A.** (1999). Dynactin is required for microtubule anchoring at centrosomes. *J. Cell Biol.* **147**, 321-334. doi:10.1083/jcb.147.2.321
- Rathbun, L., Aljiboury, A. A., Bai, X., Manikas, J., Amack, J. D., Bembenek, J. N. and Hehnl, H.** (2020). PLK1-and PLK4-mediated asymmetric mitotic centrosome size and positioning in the early zebrafish embryo. *Curr. Biol.* **30**, 4519-4527. doi:10.1016/j.cub.2020.08.074
- Reichmann, J., Nijmeijer, B., Hossain, M. J., Eguren, M., Schneider, I., Politi, A. Z., Roberti, M. J., Hufnagel, L., Hiragi, T. and Ellenberg, J.** (2018). Dual-spindle formation in zygotes keeps parental genomes apart in early mammalian embryos. *Science* **361**, 189-193. doi:10.1126/science.aar7462
- Rossi, A., Kontarakis, Z., Gerri, C., Nolte, H., Höpfer, S., Krüger, M. and Stainier, D. Y. R.** (2015). Genetic compensation induced by deleterious mutations but not gene knockdowns. *Nature* **524**, 230-233. doi:10.1038/nature14580
- Schatten, G.** (1994). The centrosome and its mode of inheritance: The reduction of the centrosome during gametogenesis and its restoration during fertilization. *Dev. Biol.* **165**, 299-335. doi:10.1006/dbio.1994.1256
- Schatten, H., Schatten, G., Mazia, D., Balczon, R. and Simerly, C.** (1986). Behavior of centrosomes during fertilization and cell division in mouse oocytes and in sea urchin eggs. *Proc. Natl Acad. Sci. USA* **83**, 105-109. doi:10.1073/pnas.83.1.105
- Schatten, H., Thompson-Coffe, C., Coffe, G., Simerly, C. and Schatten, G.** (1989). Centrosomes, centrioles, and posttranslationally modified  $\alpha$ -tubulins during fertilization. In *Molecular Biology of Fertilization* (ed. H. Schatten and G. Schatten), pp. 189-210. Academic Press.
- Schnackenberg, B. J., Khodjakov, A., Rieder, C. L. and Palazzo, R. E.** (1998). The disassembly and reassembly of functional centrosomes in vitro. *Proc. Natl. Acad. Sci. USA* **95**, 9295-9300. doi:10.1073/pnas.95.16.9295
- Silva, E., Beteja, E., John, E., Spear, P., Moresco, J. J., Zhang, S., Yates, J. R., Mitchell, B. J. and Mahjoub, M. R.** (2016). Ccdc11 is a novel centriolar satellite protein essential for ciliogenesis and establishment of left-right asymmetry. *Mol. Biol. Cell* **27**, 48-63. doi:10.1091/mbc.E15-07-0474
- Staples, C. J., Myers, K. N., Beveridge, R. D. D., Patil, A. A., Lee, A. J. X., Swanton, C., Howell, M., Boulton, S. J. and Collis, S. J.** (2012). The centriolar satellite protein Cep131 is important for genome stability. *J. Cell Sci.* **125**, 4770-4779. doi:10.1242/jcs.104059
- Stearns, T. and Kirschner, M.** (1994). In vitro reconstitution of centrosome assembly and function: the central role of gamma-tubulin. *Cell* **76**, 623-637. doi:10.1016/0092-8674(94)90503-7
- Stowe, T. R., Wilkinson, C. J., Iqbal, A. and Stearns, T.** (2012). The centriolar satellite proteins Cep72 and Cep290 interact and are required for recruitment of BBS proteins to the cilium. *Mol. Biol. Cell* **23**, 3322-3335. doi:10.1091/mbc.e12-02-0134
- Sutovsky, P. and Schatten, G.** (1999). Paternal contributions to the mammalian zygote: fertilization after sperm-egg fusion. *Int. Rev. Cytol.* **195**, 1-65. doi:10.1016/S0074-7696(08)62703-5
- Szklarczyk, D., Franceschini, A., Wyder, S., Forslund, K., Heller, D., Huerta-Cepas, J., Simonovic, M., Roth, A., Santos, A., Tsafou, K. P. et al.** (2015). STRING v10: protein-protein interaction networks, integrated over the tree of life. *Nucleic Acids Res.* **43**, D447-D452. doi:10.1093/nar/gku1003
- Szollasi, D., Calarco, P. and Donahue, R.** (1972). Absence of centrioles in the first and second meiotic spindles of mouse oocytes. *J. Cell Sci.* **11**, 521-541. doi:10.1242/jcs.11.2.521
- Sztal, T. E., McKaige, E. A., Williams, C., Ruparella, A. A. and Bryson-Richardson, R. J.** (2018). Genetic compensation triggered by actin mutation prevents the muscle damage caused by loss of actin protein. *PLoS Genet.* **14**, e1007212. doi:10.1371/journal.pgen.1007212
- Tran, L. D., Hino, H., Quach, H., Lim, S., Shindo, A., Mimori-Kiyosue, Y., Mione, M., Ueno, N., Winkler, C., Hibi, M. et al.** (2012). Dynamic microtubules at the vegetal cortex predict the embryonic axis in zebrafish. *Development* **139**, 3644-3652. doi:10.1242/dev.082362
- Woodruff, J. B.** (2018). Assembly of mitotic structures through phase separation. *J. Mol. Biol.* **430**, 4762-4772. doi:10.1016/j.jmb.2018.04.041

- Woodruff, J. B., Gomes, B. F., Widlund, P. O., Mahamid, J., Honigmann, A. and Hyman, A. A.** (2017). The centrosome is a selective condensate that nucleates microtubules by concentrating tubulin. *Cell* **169**, 1066-1077. doi:10.1016/j.cell.2017.05.028
- Woolley, D. M. and Fawcett, D. W.** (1973). The degeneration and disappearance of the centrioles during the development of the rat spermatozoon. *Anat. Rec.* **177**, 289-301. doi:10.1002/ar.1091770209
- Yabe, T., Ge, X. and Pelegri, F.** (2007). The zebrafish maternal-effect gene cellular atoll encodes the centriolar component sas-6 and defects in its paternal function promote whole genome duplication. *Dev. Biol.* **312**, 44-60. doi:10.1016/j.ydbio.2007.08.054
- Young, A., Dichtenberg, J. B., Purohit, A., Tuft, R. and Doxsey, S. J.** (2000). Cytoplasmic dynein-mediated assembly of pericentrin and  $\gamma$  tubulin onto centrosomes. *Mol. Biol. Cell* **11**, 2047-2056. doi:10.1091/mbc.11.6.2047
- Zhu, P., Ma, Z., Guo, L., Zhang, W., Zhang, Q., Zhao, T., Jiang, K., Peng, J. and Chen, J.** (2017). Short body length phenotype is compensated by the upregulation of nidogen family members in a deleterious nid1a mutation of zebrafish. *J. Genet. Genomics* **44**, 553-556. doi:10.1016/j.jgg.2017.09.011
- Zimmerman, W. and Doxsey, S. J.** (2000). Construction of centrosomes and spindle poles by molecular motor-driven assembly of protein particles. *Traffic* **1**, 927-934. doi:10.1111/j.1600-0854.2000.11202.x



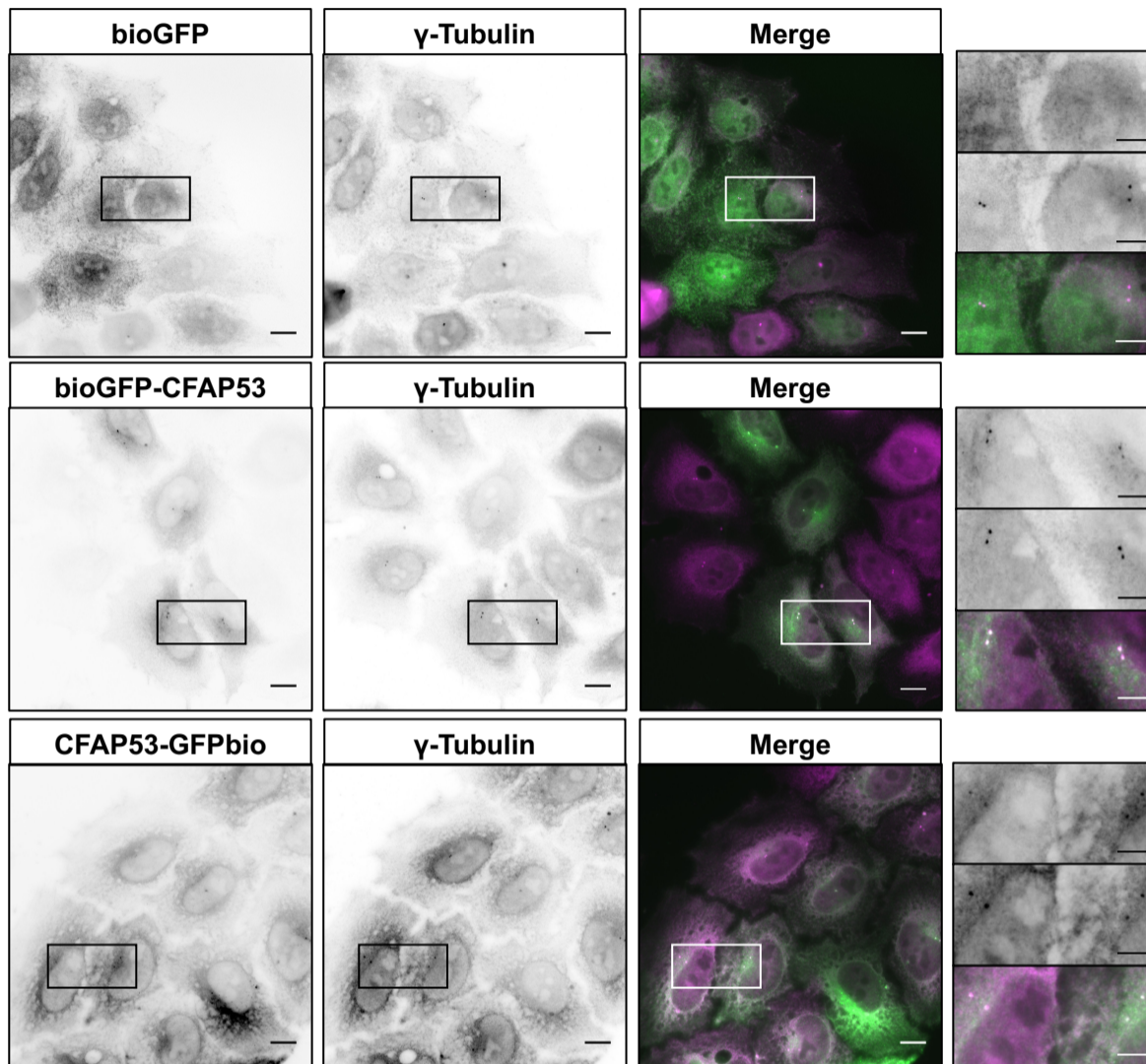


**Fig. S1. GFP-CFAP53 localization in HeLa transfected cells.** bioGFP-CFAP53 and CFAP53-GFPbio colocalize with  $\gamma$ -tubulin in transfected HeLa cells (n=25 for each construct).

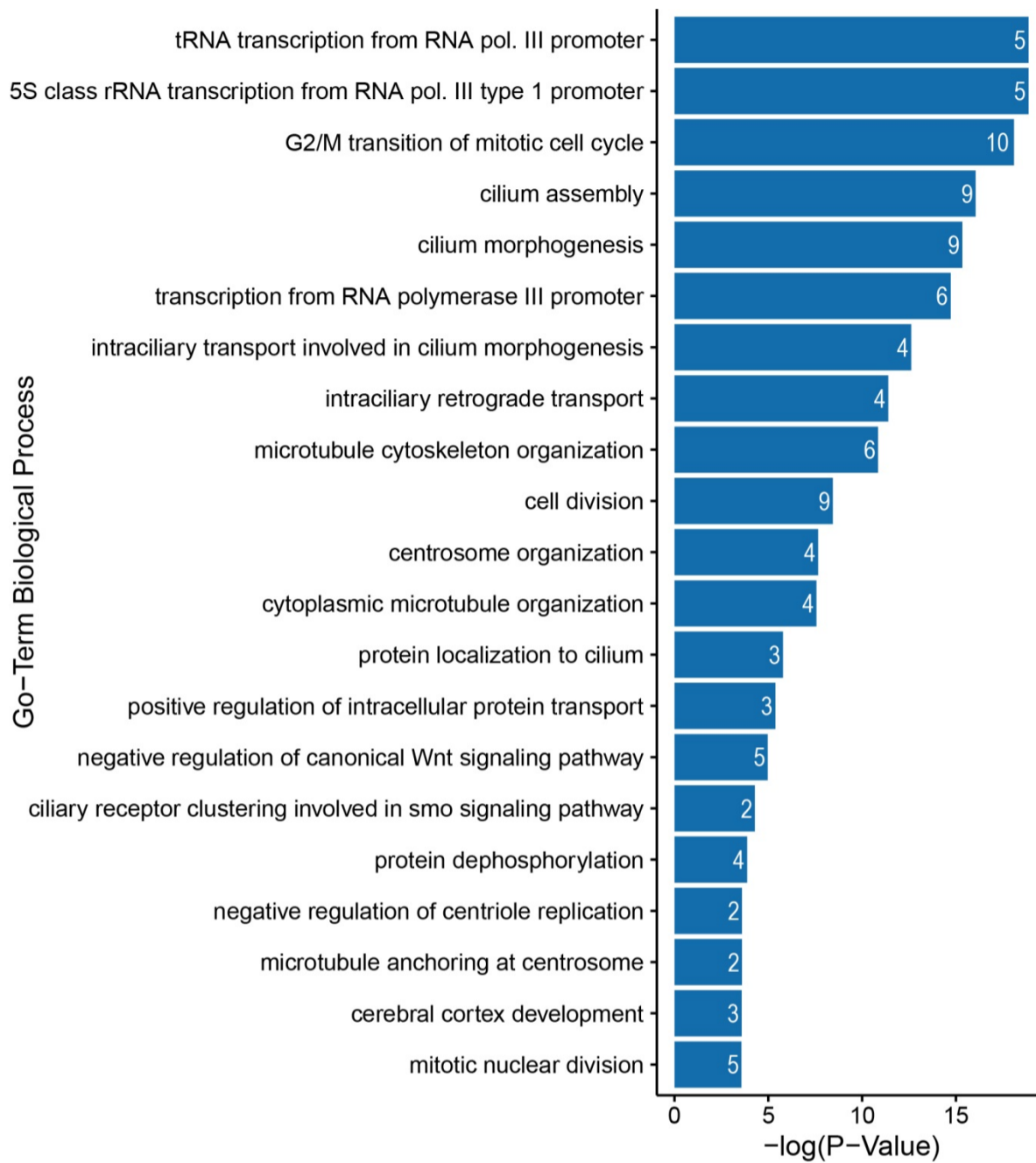


**Fig. S2. Functional GO analysis reveals a high overrepresentation of centrosomal, microtubule and cell cycle related biological processes.** High confident hits from the MS data set were selected and analyzed using DAVID thereby indicating highly enriched GO-Term biological processes in our MS data set (Huang et al., 2009; Sherman and Lempicki, 2009). Cutoff p-value < 0.03.

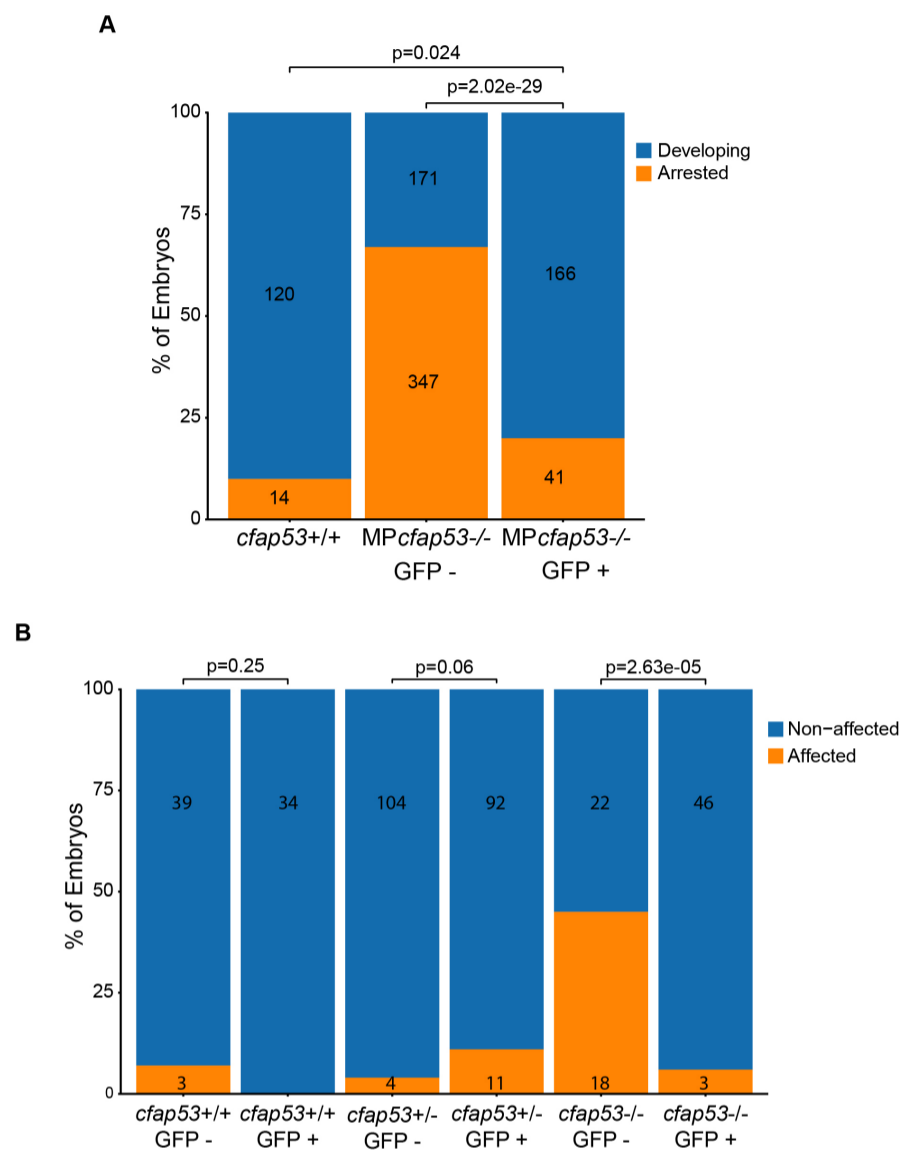


**Fig. S3. GFP-Cfap53 is a fully functional fusion protein.** (A) Barplot indicating the number of developing and arrested embryos of clutches derived from wildtype, MP*cfap53*<sup>-/-</sup> or Tg(*ubi:GFP-Cfap53*)/MP*cfap53*<sup>-/-</sup> embryos analyzed at 45 mpf. Chi-squared test was used to test for significance (p-value  $\leq 0.05$ ).

(B) Barplot indicating the distribution of embryos from an incross of *cfap53* heterozygous carriers with the Tg(*ubi:GFP-Cfap53*) that have affected laterality. Embryos with cardiac laterality defect (either right jogging or no jogging) were categorized as affected. Embryos with normal cardiac laterality (left jogging) were categorized as non-affected. Heart jogging and Cfap53-GFP expression was scored 26 hours after fertilization. As cardiac laterality is randomized in *cfap53*<sup>-/-</sup> embryos, only half of the mutant embryos are affected. P-value is generated from a test of independence (Fisher's Exact test). Numbers in bars indicate the number of embryos analysed from at least two independent matings.



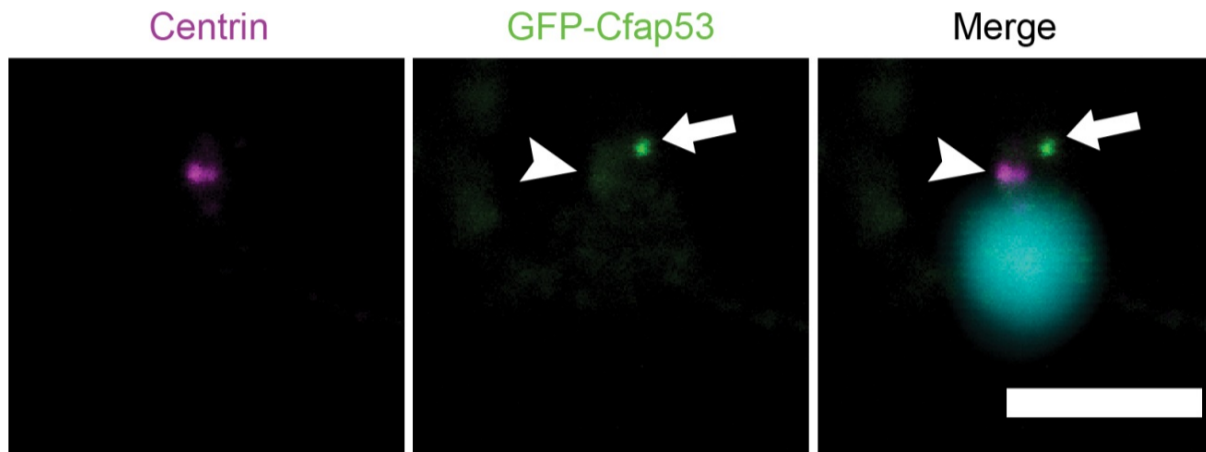


**Fig. S4. GFP-Cfap53 localization in sperm.** Centrin and GFP immunolabeling in fixed zebrafish sperm cells. In the merge DAPI is shown in cyan. Arrowhead indicates weak GFP-Cfap53 signal that colocalizes with Centrin. Arrow indicates strong signal of GFP-Cfap53 localizing in an uncharacterized structure in the sperm cell (n = 30 out of total 40 sperm cells analyzed in total). Scalebar indicates 5 microns.

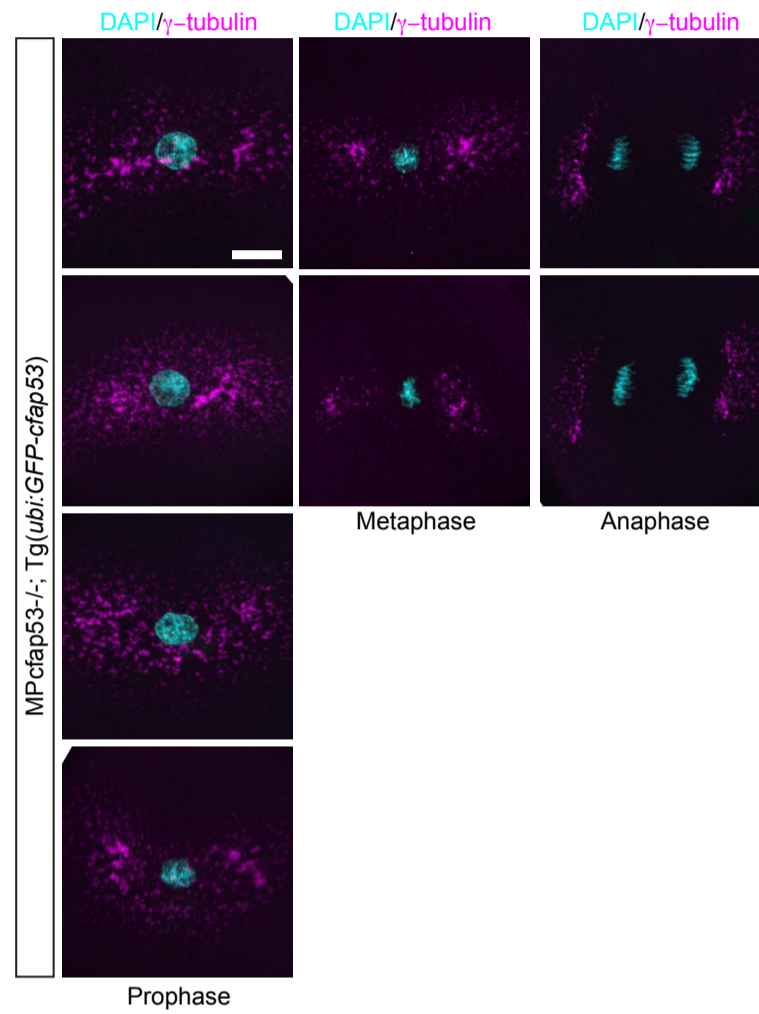


**Fig. S5. Cfap53 is important for the first cell division.**

Maximal projections of confocal stacks from fixed MPcfap53<sup>-/-</sup>;Tg(ubi:GFP-cfap53) embryos immunolabeled for  $\gamma$ -tubulin and DAPI at 45 mpf.  $\gamma$ -tubulin shows normal localization and chromosomes segregate normally during anaphase.

**Table S1. Computer-assisted sperm analysis (CASA) of wild type and Cfap53 -/- sperm cells.**

	Fish ID	Genotype	Total number of sperm cells	% Motile sperm cells
	2	mu	2606	76.5
	4	mu	1027	84.5
	6	mu	414	83.1
	8	mu	990	84.9
	10	mu	2432	78.9
	12	mu	2043	86.0
	14	mu	1450	85.5
<b>Mean</b>			1566	83.0
<b>SD</b>			819	4.0
	1	wt	1432	58.2
	3	wt	381	61.9
	5	wt	1052	87.1
	7	wt	2492	88.4
	9	wt	4981	83.5
	11	wt	1689	84.0
	13	wt	3565	87.8
<b>Mean</b>			2227	79
<b>SD</b>			1589	13
<b>T-test (p-value)</b>			0.347	0.437



**Table S2: High confidence hits from GFP-CFAP53 and CFAP53-GFP AF-MS analysis.**

Accession	gene name	Score BirA	Score GFP-Cfap53	Score Cfap53-GFP	FCA score	FCA>=7	FCB score	FCB>=3	SAINT probability	SAINT>=0.95
Q9Y5B8	NME7		9712.88	9373.19	195.86	TRUE	105	TRUE	1	TRUE
Q15154	PCM1		4291.57	6558.99	145.35	TRUE	22.58	TRUE	1	TRUE
O15078	CEP290		3566.09	4333.98	136.39	TRUE	82.03	TRUE	1	TRUE
Q12789	GTF3C1		1472.83	5518.23	112.92	TRUE	19.37	TRUE	1	TRUE
Q96M91	CFAP53	232.85	73292.73	52087.98	77.77	TRUE	186.39	TRUE	1	TRUE
Q14999	CUL7		3572.68	2817.23	75.71	TRUE	36.12	TRUE	1	TRUE
Q6P5Z2	PKN3		4494.97	1531.99	74.23	TRUE	39.55	TRUE	1	TRUE
Q8N4C6	NIN		2964.33	1122.01	66.11	TRUE	20.99	TRUE	1	TRUE
Q9Y2I6	NINL		1668.40	1813.86	62.64	TRUE	37.82	TRUE	1	TRUE
O94972	TRIM37		1930.66	915.02	51.14	TRUE	30.32	TRUE	1	TRUE
Q2M1P5	KIF7		1343.00	1718.19	49.87	TRUE	30.27	TRUE	1	TRUE
Q9UG01	IFT172		1476.88	1245.93	47.08	TRUE	20.13	TRUE	1	TRUE
A1XBS5	FAM92A1		2409.88	2791.52	44.58	TRUE	27.1	TRUE	1	TRUE
Q92621	NUP205	34.08	2351.65	3213.88	44.07	TRUE	7.71	TRUE	1	TRUE
Q9Y5Q9	GTF3C3		1317.28	2326.24	43	TRUE	8.85	TRUE	1	TRUE
Q9Y2K1	ZBTB1		1866.79	1530.88	40.22	TRUE	24.46	TRUE	1	TRUE
Q9Y5Q8	GTF3C5		666.78	1521.12	36.45	TRUE	9.07	TRUE	1	TRUE
Q9UKN8	GTF3C4		527.51	2123.97	33.64	TRUE	8.32	TRUE	1	TRUE
Q07864	POLE		428.18	1328.73	29.92	TRUE	10.67	TRUE	1	TRUE
Q96RY7	IFT140		888.15	658.20	29.03	TRUE	17.21	TRUE	1	TRUE
Q5TB80	CEP162		1131.49	472.55	28.72	TRUE	16.74	TRUE	1	TRUE
Q6ZU80	CEP128		622.24	506.35	28.4	TRUE	17.34	TRUE	1	TRUE
A6NKD9	CCDC85C		1361.54	787.12	28.1	TRUE	16.68	TRUE	1	TRUE
Q96C92	SDCCAG3		2080.95	1198.38	27.48	TRUE	13.04	TRUE	1	TRUE
O60318	MCM3AP		732.66	521.26	27.46	TRUE	13.31	TRUE	1	TRUE
Q9Y5P8	PPP2R3B		877.37	945.72	25.59	TRUE	15.72	TRUE	1	TRUE
Q9H6D7	HAUS4		1016.32	555.32	24.99	TRUE	6.91	TRUE	1	TRUE
Q9NVR7	TBCCD1		913.02	993.49	24.97	TRUE	15.34	TRUE	1	TRUE
Q13395	TARBP1		1281.56	480.86	24.37	TRUE	10.25	TRUE	1	TRUE
O95714	HERC2		198.09	748.55	23.08	TRUE	13.01	TRUE	1	TRUE
Q15058	KIF14		569.83	417.42	22.8	TRUE	5.48	TRUE	1	TRUE
Q9Y3M2	CBY1		1311.47	1305.70	22.79	TRUE	14.04	TRUE	1	TRUE
Q8TCG1	KIAA1524		932.99	516.93	20.93	TRUE	12.58	TRUE	1	TRUE
Q96JN8	NEURL4		613.28	817.72	20.92	TRUE	12.88	TRUE	1	TRUE
Q8WUA4	GTF3C2		182.82	1341.30	20.89	TRUE	7.15	TRUE	1	TRUE
O60232	SSSCA1		2125.04	293.58	20.64	TRUE	7.06	TRUE	1	TRUE
Q8NB25	FAM184A		728.91	408.52	20.63	TRUE	12.13	TRUE	1	TRUE
Q8TD10	MIPOL1		1092.86	565.77	20.31	TRUE	12.36	TRUE	1	TRUE

Q5SW79	CEP170		421.99	711.24	20.29	TRUE	3.67	TRUE	1	TRUE
Q9UL15	BAG5		1244.28	518.88	20.01	TRUE	9.23	TRUE	1	TRUE
Q53T94	TAF1B		625.19	1085.98	19.67	TRUE	12.09	TRUE	1	TRUE
Q9BV73	CEP250		568.26	385.68	19.37	TRUE	10.49	TRUE	1	TRUE
Q9UPN4	CEP131		494.31	455.41	19.36	TRUE	6.99	TRUE	1	TRUE
O14802	POLR3A		320.47	364.56	17.8	TRUE	6.13	TRUE	1	TRUE
Q86VW0	SESTD1		766.52	500.12	17.5	TRUE	10.87	TRUE	1	TRUE
P42695	NCAPD3		230.42	664.25	17.17	TRUE	7.04	TRUE	1	TRUE
Q7Z4Q2	HEATR3		603.73	494.12	16.56	TRUE	9.48	TRUE	1	TRUE
Q13136	PPFIA1		564.86	442.51	16.26	TRUE	7.98	TRUE	1	TRUE
Q7Z7A1	CNTRL		591.36	194.10	15.96	TRUE	8.23	TRUE	1	TRUE
Q96CS2	HAUS1		892.15	247.33	15.95	TRUE	8.72	TRUE	1	TRUE
Q12923	PTPN13		298.28	606.29	15.93	TRUE	9.6	TRUE	1	TRUE
Q15834	CCDC85B		523.45	259.31	15.33	TRUE	9.31	TRUE	1	TRUE
O94964	SOGA1		127.53	597.99	14.99	TRUE	6.44	TRUE	1	TRUE
Q92574	TSC1		829.10	229.59	14.71	TRUE	8.04	TRUE	1	TRUE
Q8N3Y1	FBXW8		608.23	810.83	14.69	TRUE	9.08	TRUE	1	TRUE
Q709F0	ACAD11		520.08	599.16	14.69	TRUE	9.08	TRUE	1	TRUE
Q96SN8	CDK5RAP2		297.33	346.72	14.39	TRUE	8.04	TRUE	1	TRUE
Q9NQC7	CYLD		512.00	183.38	13.77	TRUE	8.59	TRUE	1	TRUE
Q9UL42	PNMA2		579.18	357.88	13.77	TRUE	8.3	TRUE	1	TRUE
Q8NEZ3	WDR19		356.13	233.78	13.45	TRUE	8.42	TRUE	1	TRUE
P42345	MTOR		169.75	178.28	13.14	TRUE	4.12	TRUE	1	TRUE
Q86SQ0	PHLDB2		549.97	177.69	12.53	TRUE	7.06	TRUE	1	TRUE
Q9H1A4	ANAPC1		235.49	245.08	11.89	TRUE	7.5	TRUE	1	TRUE
Q8IWT3	CUL9		650.78	583.43	11.89	TRUE	4.92	TRUE	1	TRUE
P23258	TUBG1		509.59	288.73	11.59	TRUE	4.89	TRUE	1	TRUE
Q7Z494	NPHP3		594.04	26.64	11.29	TRUE	4.68	TRUE	1	TRUE
Q8TED0	UTP15		131.05	455.84	10.95	TRUE	5.61	TRUE	1	TRUE
Q7Z4L5	TTC21B		254.32	147.79	10.66	TRUE	6.46	TRUE	1	TRUE
P07199	CENPB		519.75	331.42	10.35	TRUE	3.32	TRUE	1	TRUE
Q06190	PPP2R3A		290.99	276.44	10.34	TRUE	6.59	TRUE	1	TRUE
Q9UPU5	USP24		376.51	133.43	10.03	TRUE	4.36	TRUE	1	TRUE
Q96GE4	CEP95		316.56	288.25	10.02	TRUE	6.38	TRUE	1	TRUE
Q9HD67	MYO10		201.65	201.65	9.71	TRUE	6.21	TRUE	1	TRUE
Q9C099	LRRCC1		215.78	89.83	9.42	TRUE	4.89	TRUE	1	TRUE
Q9HBG6	IFT122		264.23	136.12	8.47	TRUE	5.36	TRUE	1	TRUE
Q9BWT7	CARD10		153.06	119.83	8.16	TRUE	5.26	TRUE	1	TRUE
Q15029	EFTUD2		181.21	282.05	8.15	TRUE	4.23	TRUE	1	TRUE
Q8WV44	TRIM41		64.95	368.58	8.15	TRUE	3.31	TRUE	1	TRUE
A1A4S6	ARHGAP10		382.43	32.38	7.86	TRUE	3.84	TRUE	1	TRUE
P14373	TRIM27		283.78	223.57	7.85	TRUE	3.36	TRUE	1	TRUE

Q9Y4C2	TCAF1		240.29	169.07	7.54	TRUE	4.91	TRUE	1	TRUE
Q5JTC6	AMER1		283.72	214.16	7.54	TRUE	3.67	TRUE	1	TRUE
Q8NCN5	PDPR		308.17	126.01	7.23	TRUE	4.73	TRUE	1	TRUE
Q06481	APLP2		275.02	113.53	7.23	TRUE	4.67	TRUE	1	TRUE
O00743	PPP6C		219.78	106.47	7.23	TRUE	4.59	TRUE	1	TRUE
Q9GZT3	SLIRP		270.85	142.26	7.23	TRUE	4.35	TRUE	1	TRUE
Q96RT7	TUBGCP6		237.52	201.74	7.23	TRUE	3.97	TRUE	1	TRUE
P51530	DNA2		153.36	178.44	7.22	TRUE	4.71	TRUE	1	TRUE



**Table S3. Overlap of identified proteins in this study compared to two centriolar satellite proteomic studies.**

	Overlap with this study (%)
<b>Quarantotti et al., 2019</b>	28
<b>Gheigratmand et al., 2019</b>	38

Overlapping proteins with this study	
Quarantotti et al. 2019	Gheigratmand et al., 2019
PCM1	NME7
CEP290	PCM1
NIN	CEP290
TRIM37	NIN
KIF7	NINL
CEP162	TRIM37
CEP128	KIF7
PPP2R3B	CEP128
HAUS4	SDCCAG3
HERC2	MCM3AP
KIF14	HAUS4
CBY1	HERC2
FAM184A	KIF14
CEP170	KIAA1524
CEP250	NEURL4
CEP131	FAM184A
CNTRL	MIPOL1
HAUS1	BAG5
ACAD11	CEP250
CDK5RAP2	CEP131
CYLD	PPFIA1
TUBG1	HAUS1
CEP95	PTPN13
LRRCC1	SOGA1
TRIM41	TSC1
	CDK5RAP2
	CYLD
	PHLDB2
	PPP2R3A
	CEP95
	LRRCC1
	TRIM41
	TRIM27